Science Advances
AAAS

Manuscript Template

FRONT MATTER

Title

- Concentration-dependent transcriptional switching through a collective action of cis-elements
- Cis-element mediated transcriptional switching

Authors

Kevin Rodriguez [1, †] , Albert Do [1, †], Betul Senay-Aras [2,3, †], Mariano Perales [1], Mark Alber [2,3], Weitao Chen [2,3, *], G. Venugopala Reddy[1,3, *]

Affiliations

[1] Department of Botany and Plant Sciences, University of California Riverside, Riverside, CA 92521.

[2] Department of Mathematics, University of California Riverside, Riverside, CA 92521.

[3] Interdisciplinary Center for Quantitative Modeling in Biology, University of California Riverside, Riverside CA 92521.

† Authors contributed equally to this work.

Correspondence to: * G. Venugopala Reddy (venug@ucr.edu) and *Weitao Chen (weitaoc@ucr.edu)

Abstract

Gene expression specificity of Homeobox transcription factors has remained paradoxical. WUSCHEL activates and represses *CLAVATA3* transcription at lower and higher concentrations, respectively. We employ computational modeling and experimental analysis to investigate the properties of the Cis-regulatory module. We find that intrinsically each cis-element can only activate *CLAVATA3* at a higher WUSCHEL concentration. However, together they repress *CLAVATA3* at higher WUSCHEL and activate only at lower WUSCHEL, showing that the concentration-dependent interactions among cis-elements regulate both activation and repression. Biochemical experiments show that two adjacent functional cis-elements bind WUSCHEL with higher affinity and dimerize at relatively lower levels. Moreover, increasing the distance between cis-elements prolongs WUSCHEL monomer binding window resulting in higher *CLAVATA3* activation. Our work showing a constellation of optimally-spaced cis-elements of defined affinities determining activation and repression thresholds in regulating *CLAVATA3* transcription provides a new mechanism of co-factor independent regulation of transcription factor binding in mediating gene expression specificity.

Teaser

WUSCHEL concentration-dependent transcriptional switching by optimally spaced cis-elements of defined number and affinities.

MAIN TEXT

Introduction

Spatio-temporal regulation of gene expression is critical for specifying different cell types during development (*1-3*). Eukaryotic gene regulation involves interactions among DNA sequences and proteins, many of which are transcription factors. Enhancers, the DNA sequences that bind a given transcription factor (TF) or multiple TFs, can regulate transcription irrespective of their location in the gene (*1, 3, 4*). Since a given class of TFs binds similar DNA sequences, how they achieve gene expression specificity has been the subject of intense investigation. One of the possible mechanisms to achieve specificity is the binding of co-factors that may unmask latent binding specificity of TFs as shown in the case of Homeobox (HOX)-mediated regulation in anterior-posterior body patterning in *Drosophila melanogaster* (*5*). Another mechanism involves the utilization of the cis-regulatory modules (CRMs), a subset of enhancers that contain cis-elements for one or more TFs, which have been shown to determine the expression of neighboring genes in a variety of organisms (*4, 6-9*). In general, the CRMs can be classified into homotypic, where they bind a given type of TF, or heterotypic, where they bind different TFs (*10, 11*). The heterotypic CRMs largely have been thought to mediate spatio-temporal regulation of gene expression through their ability to recruit different collections of TFs in space and time (*10, 12, 13*).

Both the homotypic and heterotypic CRMs have been shown to regulate spatio-temporal gene expression patterns in response to TF gradients. The earliest examples of homotypic CRMs have been described in the promoters of genes activated by the TFs that accumulate in a graded manner during early embryonic development in *Drosophila* (*14-17*). Classically, the French flag model proposed by Wolpert has been applied to explain the expression of genes by TF gradients. According to this model, the target gene expression is highest in places of the highest concentration of the TF (*18*). Analysis of multiple CRMs has identified three recurring properties: cis-element number, affinity, and cooperativity, which determine gene expression (*16*). Essentially, decreasing any of the three CRM properties reduces the mean expression while increasing any of the properties leads to overexpression (*15, 16, 19, 20*).

In *Arabidopsis* shoot apical meristems (SAMs), WUSCHEL (WUS) is a homeodomain TF expressed in the rib meristem (RM) (*21, 22*). WUS protein migrates into the overlying central zone (CZ), where it promotes stem cell fate by repressing differentiation and also activates its own negative regulator-*CLAVATA3 (CLV3)* (*23, 24*) (Fig. 1A-C). CLV3 encodes a secreted peptide that activates a receptor kinase pathway to restrict *WUS* expression (*25, 26*). WUS has also been shown to bind to the promoters of key differentiation promoting TFs to repress transcription (*27*). How the same TF activates some genes, such as *CLV3,* and represses other genes in the same cells is largely unknown. However, a recent study has provided some clues to this regulation. Perales et al. (*24*), showed that WUS binds a CRM, a collection of five closely spaced cis-elements, in the *CLV3* enhancer region (Fig. 1D). The incremental deletion of cis-elements led to downregulation of *CLV3* in the outer layers of the CZ and misexpression in the inner layers of the RM suggesting that same cis-elements mediate activation and repression of *CLV3* at lower and higher WUS respectively. Biochemical analysis revealed that WUS binds cis-elements as monomers at lower WUS concentrations and binds as dimers/multimers with increasing WUS concentrations suggesting that dimerization/multimerization of WUS at higher levels may repress *CLV3* (Fig. 1E). The biochemical analysis also revealed that DNA promotes homodimerization (*28, 29*). Furthermore, increasing the affinity of one of the cis-elements decreased the dimerization threshold and led to the repression of *CLV3* in the CZ, supporting the hypothesis of

affinity-based concentration-dependent activation-repression of transcription in maintaining *CLV3* expression over a window of WUS levels. This concentration-dependent switching of *CLV3* transcription is unique among the homotypic CRMs studied and forms an exception to the French flag model.

Understanding how the concentration-dependent transcriptional switch is established requires understanding how the *CLV3* CRM functions as a unit. The complexity of the *CLV3* CRM regulation involving five cis-elements and the bidirectional relationship between *CLV3* and WUS can be challenging to untangle experimentally. The current experimental limitations cannot provide a direct real-time view of the actual WUS/*CLV3* molecular dynamics under precisely defined conditions. A multiscale computational model capable of simulating the binding and unbinding dynamics of WUS to all five cis-elements and *CLV3* transcription at the tissue level can be helpful in providing mechanistic insights into the WUS concentration-dependent functioning of the *CLV3* CRM.

Different approaches have been developed for studying transcription factor binding dynamics. The thermodynamic models are usually based on the occupancy of the promoter by the transcription factors, the statistical weights of possible configurations and the free energy (*30-34*). However, when multiple cis-elements with different affinities and their interactions are involved as observed in *CLV3* CRM, the number of possible configurations becomes large and it is not practical to employ the thermodynamic approach. Instead, the stochastic simulation algorithm, i.e., Gillespie algorithm where the dynamics of WUS binding and unbinding to the cis-elements can be modeled as a series of probabilistic events occurring at random time steps determined is ideal to explicitly model *CLV3* transcription.

We developed a stochastic model to simulate the WUS binding to the CRM in a single cell. The single cell model was applied to simulate WUS binding the cis-elements under different concentrations and compared the simulation output with the experimental data on tissue-level expression patterns of different cis-element mutants of *CLV3*, to investigate the roles of WUS binding affinity, distance dependent cooperativity among cis-elements, and RNA polymerase II (Pol II) recruitment in the transcription process. Subsequently the single-cell stochastic model was applied to multiple cells represented by unit spheres to develop a cell-based three-dimensional (3D) model representing the SAM. The 3D model was applied to further test the mechanisms identified in single-cell model in generating the spatial patterns of *CLV3* expression.

Using a WUS gradient consistent with the experimental data, both computational models suggested a role for residence time limit (see results section for details) of WUS monomer binding to the individual cis-elements of different affinities which have been shown to activate *CLV3* largely to a similar extent when acting alone. Beyond residence time limit, the aged WUS monomers fail to activate transcription and they are replaced with newly synthesized WUS monomers to sustain *CLV3* activation. Our experimental observations showing a correlation between higher WUS turnover and increased *CLV3* activation supports such a mechanism. When multiple cis-elements are involved, we found that the cooperative binding of WUS monomers and dimers is required to achieve correct *CLV3* activation patterns. The model simulations also suggested a nonhomogeneous cooperativity among cis-elements that depends on the intervening distance between cis-elements. The model prediction on distance dependent cooperativity was tested in

experiments by increasing the intervening distance between cis-elements which revealed an increase in *CLV3* activation. The corresponding biochemical experiments revealed that an increase in intervening distance between cis-elements increased their affinity to WUS monomers, however, did not alter the concentration at which WUS monomers switch to form stable dimers/higher molecular weight complexes. These results show the importance of optimal spacing between cis-elements in determining the concentration range over which appropriate number of WUS monomers and dimers populate on cis-elements in setting up the activation-repression thresholds. The 3D model that incorporates multiple cis-elements of different affinities that are spaced optimally, allowed independent manipulation of the monomer and dimer cooperativity. Our simulations revealed monomer cooperativity was critical for expression of *CLV3* at lower WUS concentration, while the dimer cooperativity was critical for repression at higher WUS concentration. Moreover, a balance of the monomer and dimer cooperativity levels was critical to achieve the wild-type *CLV3* expression at a WUS concentration range observed in experiments.

Results

Affinity and collective activity of multiple cis-elements determine *CLV3* expression.

Incremental mutations of cis-elements within the CRM result in incremental downregulation of *CLV3* expression in outer cell layers of the CZ and upregulation in the inner cell layers of the RM, suggesting interaction among cis-elements (*24*). To understand the collective behavior of cis-elements, we first deduced the contribution of each cis-element within the CRM to the regulation of *CLV3* by analyzing the loss of binding mutations in each of the five cis-elements. Single loss of binding mutations in high-affinity cis-element 970 (Fig. 1D, Table S1), led to drastic downregulation in the outer layers of CZ (Fig. 2A, B, Fig. S1). On the other hand, independent loss of binding mutations in the four lower affinity cis-elements led to a minor downregulation in the L1 layer (Fig. 2A, C). These results show that all five elements contribute to the *CLV3* expression, with the highest affinity cis-element contributing maximally over the lower affinity cis-elements *CLV3*. Moreover, our previous work shows that increasing the affinity of 970 cis-element alone downregulated *CLV3* expression revealing the critical role of affinity of cis-elements in regulating the *CLV3* expression (Fig. 2A, D). These results suggest that each cis-element contributes to *CLV3* expression and their affinities are critical to achieving proper spatial regulation.

Single cis-elements can only activate *CLV3* at higher WUS level

The subtle changes observed upon mutating individual lower affinity cis-elements ruled out a simple additive interaction in regulating *CLV3* expression. Therefore, to further understand the nature of interactions among cis-elements, we first determined the contribution of each one of the five cis-elements to *CLV3* expression, referred to as the intrinsic (i) behavior. We generated a library of 5 mutant *CLV3* reporters; each contained only one functional cis-element referred to as 970i, 997i, 1007i, 950i, and 1060i. The reporter expression analysis revealed a dramatic downregulation of *CLV3* expression in outer cell layers of CZ, including the higher affinity cis-element-970i (Fig. 2E, F, Fig. S1). To test further the importance of affinities in influencing intrinsic behavior, we analyzed the expression of 970M4i (Fig. 2E, H). The 970M4 cis-element is a mutation in 970 which

binds WUS with three times higher affinity, and it has been shown repress *CLV3* expression even at lower WUS in outer cell layers of CZ (*24*). The 970M4i reporter (Fig. 2E, H, Fig. S1) was expressed at a significantly higher level than the 970M4 (Fig. 2A, D). To further test whether the reactivation of *CLV3* associated with the 970M4i is functionally relevant, we examined its ability to complement *clv3-2* null mutants by expressing *CLV3* genomic version. The 970M4 mutants partially complement the SAM and the floral meristem (FM) phenotypes when compared to the wild-type *CLV3* promoter (Fig. 3, Fig. S2). However, the 970M4i was able to significantly better complement both the SAM and FM phenotypes showing the reactivation of 970M4i (Fig. 3F, l). Furthermore, both 970i (Fig. 3E, K) and 970M4i (Fig. 3F, L) complemented *clv3-2* to a similar extent despite binding WUS with different affinities. Consistent with this conclusion, all single cis-elements irrespective of large differences in their WUS binding affinities largely activated *CLV3* only in the inner layers of RM where WUS accumulates at a higher level (Fig. S3). However, cis-element affinity is important in the context of other functioning cis-elements in the CRM, as exemplified by the repression of 970-M4. In summary, the affinity-dependent collective WUS binding to all five cis-elements is required for balancing activation and repression of transcription in regulating the spatial expression and levels of *CLV3*.

Description of a stochastic single-cell model of *CLV3* transcription

To investigate the mechanisms of interaction among five cis-elements, we developed a stochastic modeling framework to simulate the WUS binding to the *CLV3* CRM in a single cell, together with the RNA Polymerase II (Pol II) recruitment and *CLV3* mRNA synthesis (Fig. 4A). The model was applied to understand the mechanisms underlying the *CLV3* activation by the individual cis-elements that bind WUS with different affinities and the interactions among multiple cis-elements in regulating the *CLV3* expression together. The stochasticity was introduced by implementing the Gillespie algorithm (*35*) to simulate all possible WUS binding and unbinding events to form a monomer or dimer and recruitment of Pol II for activating *CLV3* transcription. A sufficiently long time was allowed for all the simulations to reach the steady-state. The *CLV3* reporter analysis performed in the wild-type background, uses a steady-state WUS gradient, to quantify the effects of the number, affinity and intervening distance between cis-elements on *CLV3* expression. Since the focus of this study is to analyze concentration-dependent binding of WUS to the *CLV3* CRM, the feedback regulation of CLV3 on WUS was disabled to maintain a constant WUS concentration gradient throughout simulations to match the reporter analysis. It was also assumed that WUS binding the *CLV3* CRM alone would not change the overall WUS concentration. The stochastic time step and index for the next occurring event were generated by following the original Gillespie algorithm based on the assumption that binding to one cis-element was independent of the other cis-elements unless cooperativity among cis-elements exists. The average amount of *CLV3* mRNA synthesized, at a fixed WUS concentration, from multiple simulations was calculated. The model was then applied to measure the total amount of *CLV3* mRNA synthesized at different WUS concentrations (See Supplementary Materials for details).

Modeling WUS binding to the cis-regulatory module

Our previous analysis revealed that each cis-element binds WUS at different concentrations as monomers first and then switches to forming dimers at increasing concentrations (*24*). Therefore, we first aimed to determine the binding and unbinding

probabilities associated with each cis-element by reproducing the ratio of monomer and dimer bound cis-elements observed in Electrophoretic Mobility Shift Assay (EMSA) experiments (*24*). Since increasing the TF concentration decreases the search time of its binding to cis-elements (*36*), it was assumed that the probability of WUS binding to cis-elements increases with the increase in WUS concentration. In particular, the propensity of WUS binding to an empty cis-element or with a monomer is assumed to depend linearly on WUS concentration, i.e., $k_{on}^{M}[WUS]$, where k_{on}^{M} is the binding rate. Then the unbinding propensity k_{off}^{M} of WUS associated with each cis-element is calculated as k_{off}^{M}=$K_d^M k_{on}^{M}$, where K_d^M , the dissociation constant, was quantified in our previous work (*24*) (Table S1). To test this assumption, we considered a wide range of WUS concentration that encompasses WUS monomer and dimer binding to each one of the five cis-elements observed in EMSA experiments (*24*). We first simulated WUS monomer binding to a single cis-element to determine k_{on}^{M}, a free parameter, such that proportions of bound monomers obtained in the model were similar to those observed in the EMSA experiments with WUS that lacked the C-terminal homodimerization domain (Fig. S4A). Since dimerization occurs through sequential recruitment of WUS to the WUS monomer-DNA complex, we next modeled the dimer formation by recruiting the second WUS molecule to a monomer. In absence of the experimental values on binding affinity associated with the WUS dimerization, we chose K_d^D associated with the binding of the second WUS molecule to be the same as the one used to simulate monomer K_d^M. We chose k_{on}^{D} for dimer binding such that proportions of monomer and dimer bound to the cis-elements matched the EMSA experiments with full-length WUS (*24*) (Fig. S4B).

Modeling *CLAVATA3* transcription

We considered the recruitment of Pol II as another stochastic event in the model. It has been shown that the transition from monomer binding to dimer binding could be correlated to the transcriptional switch from activation to repression of *CLV3*. Therefore, we assumed monomer binding recruits Pol II to activate *CLV3* transcription while the WUS dimers fail to recruit Pol II and activate *CLV3* transcription. We introduced a time delay between two successive Pol II recruitment events due to the size of the Pol II complex occupying the transcription start site. The time delay calculated based on an 80 bp footprint of RNAp and mRNA elongation rate, which is estimated to be 1.2 kb/min (*37*), was approximated as $80\ bp \times \frac{60sec}{1200bp} = 4\ sec$. It is also assumed that after transcription initiation, the WUS monomer can unbind or bind another WUS molecule to form a dimer. Moreover, we considered the Pol II recruitment rate as an uncalibrated parameter and carried out perturbations to examine its effect on the transcriptional output. The model was calibrated over a wide range of WUS concentrations. We then applied the model to simulate WUS binding/unbinding to a single cis-element and Pol II recruitment to generate the intrinsic expression of *CLV3* at different WUS concentrations. By comparing the *CLV3* mRNA production with the experimental quantification of the *CLV3* expression in (Fig. 2E-H), an optimal scale of WUS concentrations was obtained to capture the WUS gradient in different cell layers of the SAM. This optimal WUS concentration scale was used in all single-cell simulations to investigate possible mechanisms controlling the intrinsic behavior of each cis-element in regulating the *CLV3* expression.

Mechanisms of the intrinsic behaviors of cis-elements in regulating *CLV3*

It has been observed that the transcriptional output depends on the affinity of cis-elements and the TF concentration (*30, 32, 38-45*). In general, a higher affinity cis-element results in a longer TF occupancy than the lower affinity cis-element at a given WUS concentration. Consequently, a longer TF occupancy leads to a higher mRNA production (*46*). Experiments reveal that WUS binds to 970M4i with approximately 21.4 times higher affinity than to the lowest affinity cis-element-1060i. Therefore, a longer residence time of WUS on 970M4i was expected to produce much higher levels of *CLV3* than 1060i. However, our experiments revealed that though 5 cis-elements bound WUS with different affinities, intrinsically (950i, 970i, 997i, 1007i and 1060i mutants), they were able to similarly activate *CLV3* only in inner cell layers of RM where WUS concentration is higher (Fig. 2E-H). The initial attempt in modeling by assuming WUS occupancy based on affinities produced distinct *CLV3* expression patterns for the highest -970M4i and the lowest -1060i cis-element (Fig. 4B). The 970M4i produced a much sharper increase in *CLV3* expression at lower WUS concentration than 1060i. With the increase in WUS concentration, the 970M4i produced a lower amount of *CLV3* mRNA which is expected due to the WUS dimerization, while the 1060i continued to yield higher *CLV3* mRNA (Fig. 4B). Such dramatically different *CLV3* expression patterns produced by 970M4i and 1060i were not consistent with experimental observations, suggesting additional mechanisms may regulate the intrinsic activation behavior of cis-elements in addition to their affinities.

It has been noticed for different types of TFs, including General Control transcription factor (GCN4) in yeast (*47*), and transcriptional co-activator-NPR1 involved in systemic acquired resistance (SAR) in *Arabidopsis* (*48*), a higher turnover of TFs leads to a higher transcriptional activation. Furthermore, the transcriptional activation domains (TADs) of GCN4 and other TFs have been shown to overlap with degradation domains, suggesting a possible correlation between transcriptional activation and TF turnover (*47, 49*). Moreover transcription-dependent degradation has been shown for SREBP family of transcription factors (*50*). These observations suggest that TFs when actively transcribing may get progressively modified (for example phosphorylated) and become transcriptionally ineffective and marked for their degradation (*47, 49*). Although deep mechanistic links between WUS, protein phosphorylation and protein destabilization machinery are still unknown, our earlier work suggests similarities between WUS and TFs described above. a) The transcriptional regulatory domains (WUS-box and EAR-like domains) function as degrons (*51, 52)*. b) The *CLV3* activated at lower WUS concentration in the CZ can be repressed by enriching and stabilizing the WUS protein in the nucleus (*24, 51*). c) The Dexamethasone (Dex)-mediated nuclear translocation of WUS by using the 35S::eGFP-WUS-GR system led to an immediate destabilization of the protein in the CZ within 6hrs (*53*). By 24hrs of Dex application, the protein was only detected in the nuclei of cells in the edge of the PZ and deeper cell layers of the RM. The *CLV3* activation and expansion into the PZ followed the centripetal pattern of rapid destabilization of the WUS protein (*53*; Fig. 5).

Perhaps degradation of WUS decreases the dimer concentration or creates a dynamic WUS that works favorably with the Pol II binding limit to increase *CLV3* activation. Therefore, we considered an upper limit on the residence time of WUS beyond which WUS becomes inactive and fails to recruit Pol II, referred to as residence time limit in the model (Fig. 4A). The older/inactive WUS species need to be replaced with newly synthesized WUS monomers to maintain transcription. Therefore, we imposed the same WUS monomer residence time limit for all cis-elements. A drastically lower WUS

monomer residence time limit substantially decreased *CLV3* expression for all cis-elements (Fig. 4C, S5). Simulations with a balanced residence time limit were able to generate a similar intrinsic expression pattern of *CLV3* for all cis-elements. In particular, to generate similar expression patterns of 970M4i (highest affinity) and 1060i (lowest affinity) cis-elements, we chose the residence time limit to be 10 for all simulations involving multiple cis-elements discussed in the following sections (Fig. 4B-D, Fig. S5).

The *CLV3* CRM composition determines sensitivity to dynamic changes in WUS protein levels

The number of cis-elements may also determine the sensitivity of the *CLV3* promoter to WUS levels to regulate spatial expression of *CLV3*. To test this, we analyzed the response of the mutant promoters lacking several WUS binding cis-elements to *35S::eGFP-WUS-GR* system, upon 24 hours of Dex application, described in the previous section. The wild-type *CLV3* promoter with five functional cis-elements expressed at high levels and the promoter activity expanded into the PZ (Fig. 5D, G). The mutant promoter lacking the two functional WUS binding cis-elements (970M and 997M)-*pCLV3(DM)::H2b-mYFP* is initially expressed in the deeper cell layers, and the expression levels are below that of the wild-type promoter (Fig. 5E). The 24hrs Dex application was able to activate *pCLV3(DM)* in the CZ weakly but failed to expand into the PZ (Fig. 5H) [n=8] when compared to the wild-type promoter, which revealed strong activation and radial expansion (Fig. 5G). The mutant promoter lacking four cis-elements (950M, 970M, 997M, and 1060M)-*pCLV3(QM)::H2b-mYFP* was expressed only in the deeper layers (Fig. 5F). After 24hrs of Dex application, the mutant promoter was mildly upregulated in deeper layers, however, it failed to activate in the CZ and expand radially into the PZ (Fig. 5I). Taken together, rapid destabilization of WUS can lead to higher *CLV3* activation which is maintained even at undetectable WUS protein levels showing that all five cis-elements working together increases the sensitivity of *CLV3*.

Cooperativity among cis-elements regulates *CLV3* expression

Our experimental analysis showing different expression patterns of *CLV3* for single cis-elements and multiple cis-elements suggested an interaction among cis-elements within the CRM (*24*). The same study also showed that an increase in cis-element affinity (970M4) resulted in a decrease in dimerization threshold and repressed *CLV3* in outer cell layers of CZ where WUS accumulates at a lower level. These observations suggested that cis-element affinity is important in the context of the multiple cis-elements, possibly in inducing cooperative interactions among WUS dimers bound to multiple cis-elements within the CRM. To understand the multiple cis-element behaviors, we utilized the calibrated single cell WUS binding model by extending it to include multiple cis-elements. Without any cooperative interactions among them, an increase in WUS concentration led to an increase in *CLV3* expression, which can be interpreted as a linear combination of intrinsic behaviors of individual cis-elements, which is not consistent with the experimental analysis (Fig. 6A). Therefore, we introduced cooperativity among cis-elements into the model. First, we considered equal cooperativity among all cis-elements irrespective of the intervening distance. As the cooperativity increased, the *CLV3* expression decreased at higher WUS concentration, which could be due to increased dimerization (Fig. 6B). Then we chose appropriate values for parameters involved in the

dimer cooperativity to obtain the highest activation of *CLV3* at a lower WUS concentration as observed in experiments. Next, we used the calibrated model with the chosen cooperativity parameters to simulate mutant *CLV3* consisting of different number of cis-elements. In particular, our experimental analysis showed a weaker downregulation of *CLV3* upon mutating any one of the four lower affinity cis-elements (950M, 997M, 1007M and 1060M) for low WUS concentration, compared to the highest affinity, i.e., 970 cis-element (970M) (Fig. 2A-C). However, in the simulations with the calibrated equal dimer cooperativity, the 950M was expressed at a much higher level than the wild-type at high WUS concentration (Fig. 6C), which was not consistent with the experimental observation, suggesting unequal cooperativity among those cis-elements in the CRM.

Next, we introduced unequal dimer cooperativity wherein the interaction between neighboring cis-elements was higher, and cooperativity decreased with increasing intervening distance (referred to as distance-dependent cooperativity). Similar kind of cooperativity was studied in thermodynamic models earlier (*54*). For simplicity, we simulated 970M and 950M expressions representing mutations in high and low-affinity cis-elements respectively. The model with distance-dependent dimer cooperativity was able to generate wild-type expression patterns. However, a similar expression behavior was observed for both 950M and 970M at lower WUS concentrations which is inconsistent with the experimental data (Fig. 6D). This suggested that the cis-element affinity influences interactions among cis-elements and the higher affinity cis-element-970 interacts differently than the lower affinity cis-elements in activating *CLV3* at lower WUS. Therefore, distance-dependent monomer cooperativity between cis-elements was considered. The monomer and dimer cooperativity were considered separately since one is responsible for activation and the other one is responsible for repression. Considering that the affinity plays a role when multiple cis-elements interact, the residence time limit associated with single cis-element was disabled. The additional WUS monomer cooperativity along with the dimer cooperativity between all cis-elements, was able to generate expected wild-type and the mutant (970M and 950M) cis-element behaviors at all WUS concentrations (Fig. 6E), showing the importance of both in regulating *CLV3* transcription.

The neighboring cis-elements influence WUS DNA-Protein complex formation

To test predictions of model simulations on the possible cooperative behavior of cis-elements, we performed EMSA with increasing concentration of WUS on probes that contain two adjacent cis-elements. We considered the two adjacent cis-elements-970 and 997 because mutating these two cis-elements has been shown to downregulate *CLV3* expression in outer cell layers of CZ and upregulate expression in the inner layers of RM (*24*). Full-length WUS at lower concentration has been shown to bind as a monomer to single cis-elements, which shifts to a dimeric complex at higher WUS concentration (*24*). We found that WUS bound the oligo that contains 970 and 997 cis-elements (Fig. 6I) at much lower concentrations than observed with the oligos of the same length that only contains one functional cis-element that is either the 970 (Fig. 6H) or 997 cis-element (Fig. 6G). In addition, the WUS shifted to form higher molecular weight complexes at much lower concentrations with the two functional cis-elements than one functional cis-element (Fig. 6I). To further test the nature of the protein and complex formation across multiple cis-elements, we tested the binding patterns of two WUS protein variants-WUS1-134 that only contained the DNA binding domain and lacked the centrally located homodimerization domain (HOD) and WUS1-208 that contains the centrally located HOD

domain. Our earlier work has shown that these fragments bind cis-elements with comparable affinities to the full-length protein (*24*). With increasing concentration of WUS1-134, a gradual switch from monomeric to the higher molecular complex was observed, which is expected as previous work has shown that the DNA binding domain also participates in dimerization (*24, 29*). While with the WUS1-208, at the same protein concentration range, we observed a faster shift from the monomer form into the higher molecular weight complex. Testing these two protein versions on a probe containing only one functional 970 cis-element revealed higher molecular complex formation at a much higher concentration (*24*). These results suggest that the second dimerization domain may facilitate interaction between WUS molecules bound to the adjacent cis-elements in promoting higher molecular WUS complex formation.

The distance between cis-elements is critical for *CLV3* expression

The cooperativity observed in gel shift assays suggests that the neighboring cis-elements increase WUS binding, possibly through protein-protein interaction facilitated by the second homodimerization domain (HOD2). To test the influence of spacing between cis-elements without reducing the number or affinity, we duplicated the sequence between neighboring cis-elements. The increased distance might reduce the interaction of WUS bound to neighboring cis-elements without affecting the intrinsic binding to each independent cis-elements. Therefore, we duplicated the intervening sequence between 970-997 and 997-1007 [Double space around 997] *pCLV3(DS-997)::H2B-mYFP*. Increasing the distance between neighboring cis-elements led to increased *CLV3* expression in all cell layers and increase in the deeper layers was much higher than the outer cell layers of CZ (Fig. 7A-C). These results suggest that the distance between cis-elements is more critical for the repression of *CLV3*, likely through the formation of large WUS complexes across neighboring cis-elements. In order to test whether the increased distance between 970 and 997 cis-elements alters the binding dynamics, we analyzed WUS binding to the oligo with duplicated sequences that doubled the distance between 970 and 997 (970--997). The full-length WUS protein could bind the oligo (970--997) at lower WUS (Fig. 7D,E). However, the transition from lower molecular weight complexes to higher molecular weight complexes occurred over a much wider WUS concentration range. Therefore, the increase in *CLV3* expression in all cell layers seen in DS-997 could be explained by the larger WUS concentration range over which it remains as a lower molecular weight complex, showing that in addition to the affinity of the cis-elements, the intervening distance is important in regulating the *CLV3* expression.

Description of a 3D cell-based model of *CLV3* transcription

The single-cell model provided insights into the WUS binding dynamics with individual cis-elements, Pol II recruitment, and minimum cooperativity mechanisms required for *CLV3* expression (Fig. S6). However, the single-cell model can only provide average expression behavior at given WUS concentrations, without considering the tissue spatial organization and the stochasticity associated with individual cells within layers of the SAM under a broader range of WUS concentrations. Therefore, we expanded our scope of study by developing a three dimensional (3D) multicellular model to capture the tissue-level spatial dynamics.

The 3D model could help quantify the establishment of the *CLV3* expression pattern throughout the tissue by simulating the stochastic single-cell model in individual cells

simultaneously at different WUS concentrations. The 3D model was constructed based on the framework used in our previous work (*27*) combined with new biological data and mechanisms identified by using the stochastic single-cell model. The computational domain consisted of a 3D matrix of unit spheres organized in a half-dome shape, corresponding to cells within the SAM from the L1 to L7 layers. At the tissue level, a spatial gradient of WUS proteins across different layers, which captured a similar fold change from deeper layers to outer layers observed in experiments (Fig. 8C, Fig. S3), was introduced and maintained at this fixed concentration throughout each simulation (Fig. 1A, 8C). In individual cells, the single-cell stochastic model was applied to simulate WUS binding with cis-elements by using the local WUS concentrations to regulate *CLV3* transcription. The same mechanisms identified by the single-cell stochastic model were implemented under wild-type and multiple cis-element mutant conditions. Each simulation was allowed to run long enough to achieve the steady-state behavior, and the parameters used in the simulations are listed in Table S3.

Analysis of *CLV3* expression and WUS complexes captured by the 3D model

Using a biologically relevant WUS gradient (Fig. 8C), *CLV3* simulations were generated under a variety of different conditions, including wild-type, four cis-elements (970M), three cis-elements (DM), and single cis-element (e.g. 970i). The behaviors of several cis-element mutants are shown in Fig. 8A-B. *CLV3* expression in wild-type was generally higher than other mutants, similar to the experimental data shown in Fig. 2A. In particular, wild-type *CLV3* activation was highest in the L1 layer and lowest in the inner layers of RM. 970M showed a higher expression in the inner layers of RM than in the outer L1 layer. Of particular interest was 970M4, in which the affinity was strengthened over the default 970 affinity, expressed at lower level in all cell layers. When simulating the mutants with a single functional cis-element in the CRM, e.g. 950i, 970i, 997i, 1007i, and 1060i, the *CLV3* expression was detected in only the inner layers of RM. Other than the minor difference in the magnitude, all single cis-element mutants expressed only in the inner cell layers (Fig. 8B), similar to the experimental results. Simulations also showed an impairment in the spatial patterns of *CLV3* expression as more cis-elements were deleted. For example, the deletion of a single lower affinity cis-element-950 (950M) had a relatively minimal effect on *CLV3* activation. (Fig. 8D). In contrast, deletion of the higher affinity cis-element-970 (970M) shifted *CLV3* expression to the inner layers (Fig. 8D). The more drastic shift in *CLV3* expression into deeper layers occurred when deleting four cis-elements (e.g. 950i or 970i) regardless of their WUS binding affinity (Fig. 8D). Therefore, the cooperativity mechanism identified by the single-cell stochastic model was able to generate the expected *CLV3* expression behavior in the 3D model.

Bi-molecular Fluorescence Complementation assays (BiFC) in plants expressing split eGFP-WUS constructs expressed from the native *WUS* promoter revealed very few fluorescent positive cells in the L3 and the L2 layers of SAMs (Fig. S7). These results show that WUS dimerizes in cells that accumulate higher levels of WUS supporting the correlation observed in biochemical analysis. However, the observed dimerization in BiFC assays does not distinguish between DNA-bound WUS complexes and unbound complexes. Moreover, it likely represents WUS complexes with cis-elements of many target genes (*27*). Therefore, we utilized the 3D model to visualize the spatiotemporal distributions of WUS complexes including monomers and dimers on the *CLV3* promoter across cell layers in SAMs (Fig. 8D). A higher concentration of WUS monomers in the outer layers of CZ and higher dimers in the inner layers of RM were observed for the

wild-type and lower affinity cis-element -950M. Deleting the 970 cis-element showed lower levels of WUS monomers in outer layers of CZ and lower levels of dimers in inner layers of RM (Fig. 8D). This suggested that the higher affinity cis-element exerts a stronger influence on *CLV3* transcription, but it was not sufficient to completely activate in the outer layers of the CZ or repress the inner layers of RM on its own, showing that cis-elements interact with each other in maintaining specific amounts of WUS monomer and dimer complexes in different layers in regulating *CLV3* expression. The 970M4 results resolved the seemingly paradoxical expression patterns of this mutant. A massive amount of WUS dimers in all layers that can explain a drastic reduction of *CLV3* expression. In contrast, both monomers and dimers accumulated at a lower level when only one cis-element was functional, showing that WUS failed to populate at higher levels on cis-elements likely due to the lack of cooperativity. Overall, the 3D model simulations showed the spatial distributions of WUS complex formation at a quantitative level in different cell layers of SAMs. The WUS complex formation could be correlated to WUS concentration in different cell layers and the affinity-dependent cooperative behavior of cis-elements in expressing *CLV3* in the CZ.

Effect of cooperativity on the spatial patterns of *CLV3* transcription

The experimental evidence suggested that the cooperativity among cis-elements is critical to achieving proper spatial patterns of *CLV3* expression. To better understand the role of cooperativity in the robust regulation of *CLV3* expression quantitatively, we imposed different levels of cooperativity between monomers or dimers for both wild-type and mutant conditions. A complete removal of cooperativity led to a higher *CLV3* expression in the inner cell layers of RM and a lower expression in outer cell layers of CZ under all conditions (Fig. 9A). In contrast, increasing cooperativity led to *CLV3* downregulation (Fig. 9C) showing that strength of cooperativity influences *CLV3* expression. Our experimental analysis shows that increasing the cis-element affinity (970M4) leads to downregulation of *CLV3* expression which could be due to a higher cooperativity among cis-elements leading to the repression. To test this hypothesis, we removed cooperativity from 970M4 which led to an increase in *CLV3* expression, and the pattern of expression resembled that of wild-type (Fig. 9A). These results show the importance of cooperativity in modulating *CLV3* expression, which in turn depends on the cis-element affinity.

Our experimental analysis also showed that decreasing the number of cis-elements leads to a decrease in *CLV3* expression in outer cell layers of CZ and an increase in inner cell layers of RM, suggesting that the number of cis-elements may also aid in inducing cooperativity. Consistent with the requirement of multiple cis-elements in mediating cooperativity, the effects of cooperativity levels on *CLV3* expression diminished with the deletions of multiple cis-elements (Fig. 9).

As shown above, removing the overall cooperativity that includes both the monomer and dimer cooperativity leads to the internalization of *CLV3*, which is not entirely consistent with the *in vivo* observed overall increase of *CLV3* expression even in the outer cell layers of *pCLV3(DS-997)* (Fig. 7B, C). Removing the overall cooperativity which also included the monomer cooperativity might have caused the downregulation of *CLV3* in outer cell layers of CZ. Therefore, we perturbed monomer and dimer cooperativity independently. At a constant dimer cooperativity, increasing monomer cooperativity alone led to a gradual increase in *CLV3* expression in outer cell layers and expression maxima shifted to outer cell layers (Fig. 10A and Fig. S8, S9). In contrast, increasing the dimer cooperativity

alone led to an overall decrease in *CLV3* expression, which was more pronounced in the inner layers of RM and a shift in the expression maxima to the outer layers of CZ (Fig. 10B and Fig. S8, S9). This suggests that *CLV3* expression is regulated through a balance between dimer and monomer cooperativity mediating the repression and activation, respectively. These simulation results could also help us to understand the experimental data, in which the increased expression of *CLV3* in all cell layers observed upon doubling the distance (DS-997) could be attributed to lower dimer cooperativity leading to derepression. Together, these results show that cooperativity plays a critical role in regulating *CLV3* expression when all five cis-elements are functional.

Discussion

A homotypic cluster of 5 cis-elements with different WUS binding affinities regulates levels and spatial expression of *CLV3*. WUS has been shown to activate and repress *CLV3* at lower and higher levels, respectively. Our work reveals that the relative affinities of each element, the number of cis-elements and intervening distance contribute to the collective effect. Moreover, the collective activity of the CRM arises not only because of the individual affinity but also because of cooperative binding of multiple neighboring cis-elements to WUS. WUS was previously shown to form a mixture of monomers, dimers, and oligomers in solution over a wide concentration range (*24*). Moreover, DNA/cis-elements have been shown to promote dimerization or multimerization of WUS over a small 2-4 fold increase in WUS level.

Our biochemical analysis presented here reveals that two adjacent cis-elements can increase the binding sensitivity of WUS at lower levels than the single cis-elements suggesting that the cis-elements cooperate in increasing the binding probability of WUS monomers which could contribute to boost activation. Our biochemical work also shows that the two cis-elements working together allows the formation of higher order WUS complexes at lower WUS levels which depends on the second homodimerization domain (Fig. 6J, K). This suggests that the second homodimerization domain may allow interaction of WUS species bound to the adjacent cis-elements in forming higher order complexes. WUS has two dimerization domains one of which is near the DNA binding domain and the other is found outside the DNA binding domain (*24*). The second dimerization domain may allow for protein-protein interaction across neighboring cis-elements which then allows for cooperative binding across the cis-elements. Our analysis also reveals that cis-element affinity plays a critical role in inducing cooperativity across cis-elements. The increased affinity of 970M4 cis-element contributed to higher cooperativity leading to the repression of *CLV3*. However, such repression requires other functional cis-elements in the CRM showing that the collective behavior arises as a result of the number of cis-elements and the WUS binding affinities. The collective behavior of a low affinity homotypic CRM has been shown to be critical in a recent study of the *Drosophila* SHAVENBABY locus. Increasing the binding affinity of one of the cis-elements resulted in a strong ectopic activation suggesting that low affinity homotypic CRMs may lead to higher specificity (*9*). Our work showing the importance of the number of cis-elements in regulating gene expression agrees with the fundamental concept of having multiple cis-elements organized in a constellation leads to gene expression specificity. However, the *CLV3* CRM regulation differs from other homotypic CRMs such SHAVENBABY locus where *CLV3* expression is regulated through a concentration-dependent activation-repression switching mechanism. The C-terminus of WUS has been shown to bind at least three proteins; HAIRYMERISTEM (HAM) (*55*), SHOOT-

MERISTEMLESS (STM) (*56*) and TOPLESS (TPL) (*57*). Earlier analysis shows that the C-terminus of WUS is not required for the regulation of DNA binding affinity and dimerization (*24*) and DNA binding specificity (*29*). Therefore, we suggest that WUS binding to the *CLV3* CRM is a cofactor independent mechanism that depends on the organization of cis-elements in the CRM. Besides *CLV3*, WUS has been shown to activate and repress several hundred genes (*27*). Our bioinformatics search for "TAAT" core containing cis-element clusters (see supplementary materials for details of the algorithm) identified multiple clusters in 152 out of 154 WUS-upregulated genes and 298 out of 303 WUS-downregulates genes (Tables S6 and S7). This resource should guide future *in vivo* analysis to refine our understanding of the relationship between CRMs and gene expression specificity.

Our analysis also shows that the interaction between cis-elements in promoting higher molecular WUS complexes also depends on the distance between cis-elements. Increasing the distance between cis-elements surprisingly decreased the WUS detection threshold suggesting that distance may also play a role in sensing WUS concentration through an unknown mechanism. This might increase the probability of WUS monomer binding to adjacent cis-elements. However, the stabilization of WUS into a higher molecular weight complexes still occurred at the same WUS levels as observed with the wild-type distance. Thus, the increase in *CLV3* expression observed upon increasing the distance could be due to increased activation and not entirely due to the reduced repression. Taken together our results show that the cis-element affinity plays a dominant role in *CLV3* repression while it appears that the system can withstand an increase in intervening distance in forming higher WUS complexes.

The computational model developed in this study allows us to recreate and, in a sense, verify the plausibility of our mechanistic explanations of experimental results. It was possible to quantify properties that are very difficult to obtain through experimental means such as the residence time of WUS on cis-elements to calibrate the model and visualization of concentration-dependent ratios of WUS monomer and dimer/higher order complexes on the *CLV3* cis-elements. The upper limit on the residence time of WUS was critical to explain individual cis-element behaviors that differ in their binding affinities. Our experimental analysis shows that a higher WUS turnover leads to a higher *CLV3* activation suggesting that older WUS species may become ineffective and may unbind. The nuclear export of WUS has been shown to play a crucial role in regulating the WUS nuclear concentration (*51*). It has also been shown that a nuclear export signal is required for WUS degradation in the cytoplasm. Perhaps the older WUS molecules that unbind are exported and degraded in the cytoplasm which may create space for newly synthesized WUS that moves into the outer layer of CZ to bind cis-elements to sustain *CLV3* activation. CLV3 has been shown to offset nuclear export of WUS which forms an additional feedback mechanism in regulating the nuclear concentration (*51*). Whether CLV3 levels also independently determine residence time of WUS by influencing its unbinding from cis-elements perhaps by regulating the WUS protein modifications remains to be explored. Nevertheless, a seamless connection involving WUS binding, unbinding, export and degradation could lead to a robust maintenance of *CLV3* transcription. However, the current model assumes a constant WUS gradient and is limited to exploring the mechanisms underlying the *CLV3* expression without considering the feedback regulations of CLV3 signaling on WUS. Our recent study developed a model involving both transcriptional and post-translational regulations of WUS by the CLV3 signaling (*51*). This model used a generic function of WUS concentration to represent the *CLV3* transcription. The model perturbations revealed the dual control of *WUS*

transcription and nuclear levels by the CLV3 signaling when coupled to the WUS concentration-dependent transcriptional activation and repression of *CLV3* leads to a robust maintenance of the WUS protein gradient. Our results show that the cis-element mutant reporter-970i was dramatically reset into the outer layers of CZ in the *clv3* null mutants complemented with the 970i genomic construct (Fig. S10A-B). Perhaps this is due to the effects of altered CLV3 signaling on the expression and nuclear accumulation of WUS establishing a new gradient. In the future, coupling the 3D stochastic model of *CLV3* transcription developed here with the CLV3 signaling model of the regulation of WUS transcription and the WUS protein dynamics should allow assessment of the influence of different properties of the *CLV3* CRM, including the number of cis-elements in regulating the robustness of the WUS gradient.

Materials and Methods

Experimental Design

Plants were grown under continuous light as described earlier in (*24*). Imaging was performed on the Zeiss 880 AIRYSCAN upright under a 40X objective. eGFP-WUS was excited at 488nm and collected with filter 495nm - 550nm. H2B-mYFP was excited at 514nm filtered with MBS 458/514/561/633 and collected with filter BP 495nm - 550nm. FM4-64 was excited at 561nm and collected with BP 570nm - 620nm.

Stochastic single-cell model and the 3D cell-based model

Description of two computational models developed in this study is provided in detail in the Supplemental Materials. Parameters used in the stochastic single-cell model can be found in Table S1, S2. Parameters used in the 3D cell-based model can be found on Table S1, S3.

Statistical Analysis

The source data associated with all experiments are presented in the additional data files. Additionally, the means, N, and P values are included within each data set.

References

1. M. Levine, Transcriptional enhancers in animal development and evolution. *Curr. Biol.* **20**, R754–63 (2010).

2. C.-T. Ong, V. G. Corces, Enhancer function: new insights into the regulation of tissue-specific gene expression. *Nat. Rev. Genet.* **12**, 283–293 (2011).

3. F. Spitz, E. E. M. Furlong, Transcription factors: from enhancer binding to developmental control. *Nat. Rev. Genet.* **13**, 613–626 (2012).

4. J. Banerji, S. Rusconi, W. Schaffner, Expression of a beta-globin gene is enhanced by remote SV40 DNA sequences. *Cell*. **27**, 299–308 (1981).

5. M. Slattery, T. Riley, P. Liu, N. Abe, P. Gomez-Alcala, I. Dror, T. Zhou, R. Rohs, B. Honig, H. J. Bussemaker, R. S. Mann, Cofactor binding evokes latent differences in DNA binding specificity between Hox proteins. *Cell*. **147**, 1270–1282 (2011).

6. G. Struhl, K. Struhl, P. M. Macdonald, The gradient morphogen bicoid is a concentration-dependent transcriptional activator. *Cell*. **57**, 1259–1273 (1989).

7. W. D. Fakhouri, A. Ay, R. Sayal, J. Dresch, E. Dayringer, D. N. Arnosti, Deciphering a

transcriptional regulatory code: modeling short-range repression in the Drosophila embryo. *Mol. Syst. Biol.* **6**, 341 (2010).

8. R. Joshi, J. M. Passner, R. Rohs, R. Jain, A. Sosinsky, M. A. Crickmore, V. Jacob, A. K. Aggarwal, B. Honig, R. S. Mann, Functional specificity of a Hox protein mediated by the recognition of minor groove structure. *Cell*. **131**, 530–543 (2007).

9. J. Crocker, N. Abe, L. Rinaldi, A. P. McGregor, N. Frankel, S. Wang, A. Alsawadi, P. Valenti, S. Plaza, F. Payre, R. S. Mann, D. L. Stern, Low affinity binding site clusters confer hox specificity and regulatory robustness. *Cell*. **160**, 191–203 (2015).

10. B. P. Berman, Y. Nibu, B. D. Pfeiffer, P. Tomancak, S. E. Celniker, M. Levine, G. M. Rubin, M. B. Eisen, Exploiting transcription factor binding site clustering to identify cis-regulatory modules involved in pattern formation in the Drosophila genome. *Proc. Natl. Acad. Sci. U. S. A.* **99**, 757–762 (2002).

11. A. P. Lifanov, V. J. Makeev, A. G. Nazina, D. A. Papatsenko, Homotypic regulatory clusters in Drosophila. *Genome Res.* **13**, 579–588 (2003).

12. S. Small, A. Blair, M. Levine, Regulation of even-skipped stripe 2 in the Drosophila embryo. *EMBO J.* **11**, 4047–4057 (1992).

13. Y. T. Ip, R. E. Park, D. Kosman, E. Bier, M. Levine, The dorsal gradient morphogen regulates stripes of rhomboid expression in the presumptive neuroectoderm of the Drosophila embryo. *Genes Dev.* **6**, 1728–1739 (1992).

14. W. Driever, C. Nüsslein-Volhard, The bicoid protein is a positive regulator of hunchback transcription in the early Drosophila embryo. *Nature*. **337**, 138–143 (1989).

15. J. Gaudet, S. E. Mango, Regulation of organogenesis by the Caenorhabditis elegans FoxA protein PHA-4. *Science*. **295**, 821–825 (2002).

16. J. Jiang, M. Levine, Binding affinities and cooperative interactions with bHLH activators delimit threshold responses to the dorsal gradient morphogen. *Cell*. **72**, 741–752 (1993).

17. S. Rowan, T. Siggers, S. A. Lachke, Y. Yue, M. L. Bulyk, R. L. Maas, Precise temporal control of the eye regulatory gene Pax6 via enhancer-binding site affinity. *Genes Dev.* **24**, 980–985 (2010).

18. L. Wolpert, Positional information and the spatial pattern of cellular differentiation. *J. Theor. Biol.* **25**, 1–47 (1969).

19. J. Jiang, D. Kosman, Y. T. Ip, M. Levine, The dorsal morphogen gradient regulates the mesoderm determinant twist in early Drosophila embryos. *Genes Dev.* **5**, 1881–1891 (1991).

20. D. S. Parker, M. A. White, A. I. Ramos, B. A. Cohen, S. Barolo, The cis-regulatory logic of Hedgehog gradient responses: key roles for gli binding affinity, competition, and cooperativity. *Sci. Signal.* **4**, ra38 (2011).

21. K. F. Mayer, H. Schoof, A. Haecker, M. Lenhard, G. Jürgens, T. Laux, Role of WUSCHEL in regulating stem cell fate in the Arabidopsis shoot meristem. *Cell*. **95**, 805–815 (1998).

22. H. Schoof, M. Lenhard, A. Haecker, K. F. X. Mayer, G. Jürgens, T. Laux, The Stem Cell

Population of Arabidopsis Shoot Meristems Is Maintained by a Regulatory Loop between the CLAVATA and WUSCHEL Genes. *Cell*. **100**, 635–644 (2000).

23. R. K. Yadav, M. Perales, J. Gruel, T. Girke, H. Jönsson, G. V. Reddy, WUSCHEL protein movement mediates stem cell homeostasis in the Arabidopsis shoot apex. *Genes Dev.* **25**, 2025–2030 (2011).

24. M. Perales, K. Rodriguez, S. Snipes, R. K. Yadav, M. Diaz-Mendoza, G. V. Reddy, Threshold-dependent transcriptional discrimination underlies stem cell homeostasis. *Proc. Natl. Acad. Sci. U. S. A.* **113**, E6298–E6306 (2016).

25. S. E. Clark, R. W. Williams, E. M. Meyerowitz, The CLAVATA1 gene encodes a putative receptor kinase that controls shoot and floral meristem size in Arabidopsis. *Cell*. **89**, 575–585 (1997).

26. U. Brand, J. C. Fletcher, M. Hobe, E. M. Meyerowitz, R. Simon, Dependence of Stem Cell Fate in Arabidopsis on a Feedback Loop Regulated by CLV3 Activity. *Science*. **289**, 617–619 (2000).

27. R. K. Yadav, M. Perales, J. Gruel, C. Ohno, M. Heisler, T. Girke, H. Jönsson, G. V. Reddy, Plant stem cell maintenance involves direct transcriptional repression of differentiation program. *Mol. Syst. Biol.* **9**, 654 (2013).

28. C. Koppermann, thesis, Universität zu Köln (2017).

29. J. Sloan, J. P. Hakenjos, M. Gebert, O. Ermakova, A. Gumiero, G. Stier, K. Wild, I. Sinning, J. U. Lohmann, Structural basis for the complex DNA binding behavior of the plant stem cell regulator WUSCHEL. *Nat. Commun.* **11**, 2223 (2020).

30. J. Reinitz, S. Hou, D. H. Sharp, Transcriptional Control in *Drosophila*. *Complexus*. **1**, 54–64 (2003).

31. M. A. Shea, G. K. Ackers, The OR control system of bacteriophage lambda. A physical-chemical model for gene regulation. *J. Mol. Biol.* **181**, 211–230 (1985).

32. X. He, M. A. H. Samee, C. Blatti, S. Sinha, Thermodynamics-based models of transcriptional regulation by enhancers: the roles of synergistic activation, cooperative binding and short-range repression. *PLoS Comput. Biol.* **6** (2010).

33. D. Chu, N. R. Zabet, B. Mitavskiy, Models of transcription factor binding: sensitivity of activation functions to model assumptions. *J. Theor. Biol.* **257**, 419–429 (2009).

34. M. S. Sherman, B. A. Cohen, Thermodynamic state ensemble models of cis-regulation. *PLoS Comput. Biol.* **8**, e1002407 (2012).

35. D. T. Gillespie, A general method for numerically simulating the stochastic time evolution of coupled chemical reactions. *J. Comput. Phys.* **22**, 403–434 (1976).

36. J. Swift, G. M. Coruzzi, A matter of time - How transient transcription factor interactions create dynamic gene regulatory networks. *Biochim. Biophys. Acta Gene Regul. Mech.* **1860**, 75–83 (2017).

37. T. O'Brien, J. T. Lis, Rapid changes in Drosophila transcription after an instantaneous heat

shock. *Mol. Cell. Biol.* **13**, 3456–3463 (1993).

38. G. K. Ackers, A. D. Johnson, M. A. Shea, Quantitative model for gene regulation by lambda phage repressor. *Proc. Natl. Acad. Sci. U. S. A.* **79**, 1129–1133 (1982).

39. H. G. Garcia, R. Phillips, Quantitative dissection of the simple repression input-output function. *Proc. Natl. Acad. Sci. U. S. A.* **108**, 12173–12178 (2011).

40. J. Gertz, E. D. Siggia, B. A. Cohen, Analysis of combinatorial cis-regulation in synthetic and genomic promoters. *Nature*. **457**, 215–218 (2009).

41. E. Segal, T. Raveh-Sadka, M. Schroeder, U. Unnerstall, U. Gaul, Predicting expression patterns from regulatory sequence in Drosophila segmentation. *Nature*. **451**, 535–540 (2008).

42. R. P. Zinzen, C. Girardot, J. Gagneur, M. Braun, E. E. M. Furlong, Combinatorial binding predicts spatio-temporal cis-regulatory activity. *Nature*. **462**, 65–70 (2009).

43. R. Amit, H. G. Garcia, R. Phillips, S. E. Fraser, Building enhancers from the ground up: a synthetic biology approach. *Cell*. **146**, 105–118 (2011).

44. E. Davidson, *The Regulatory Genome* (Academic Press, 2006).

45. H. G. Garcia, A. Sanchez, J. Q. Boedicker, M. Osborne, J. Gelles, J. Kondev, R. Phillips, Operator Sequence Alters Gene Expression Independently of Transcription Factor Occupancy in Bacteria. *Cell Rep.* **2**, 150–161 (2012).

46. C. R. Lickwar, F. Mueller, S. E. Hanlon, J. G. McNally, J. D. Lieb, Genome-wide protein–DNA binding dynamics suggest a molecular clutch for transcription factor function. *Nature*. **484**, 251–255 (2012).

47. J. R. Lipford, G. T. Smith, Y. Chi, R. J. Deshaies, A putative stimulatory role for activator turnover in gene expression. *Nature*. **438**, 113–116 (2005).

48. S. H. Spoel, Z. Mou, Y. Tada, N. W. Spivey, P. Genschik, X. Dong, Proteasome-mediated turnover of the transcription coactivator NPR1 plays dual roles in regulating plant immunity. *Cell*. **137**, 860–872 (2009).

49. F. Geng, S. Wenzel, W. P. Tansey, Ubiquitin and proteasomes in transcription. *Annu. Rev. Biochem.* **81**, 177–201 (2012).

50. A. Sundqvist, J. Ericsson, Transcription-dependent degradation controls the stability of the SREBP family of transcription factors. *Proc. Natl. Acad. Sci. U. S. A.* **100**, 13833–13838 (2003).

51. A. Plong, K. Rodriguez, M. Alber, W. Chen, G. V. Reddy, CLAVATA3 mediated simultaneous control of transcriptional and post-translational processes provides robustness to the WUSCHEL gradient. *Nat. Commun.* **12**, 1–13 (2021).

52. S. A. Snipes, K. Rodriguez, A. E. DeVries, K. N. Miyawaki, M. Perales, M. Xie, G. V. Reddy, Cytokinin stabilizes WUSCHEL by acting on the protein domains required for nuclear enrichment and transcription. *PLoS Genet.* **14**, e1007351 (2018).

53. K. Rodriguez, M. Perales, S. Snipes, R. K. Yadav, M. Diaz-Mendoza, G. V. Reddy, DNA-dependent homodimerization, sub-cellular partitioning, and protein destabilization control

WUSCHEL levels and spatial patterning. *Proc. Natl. Acad. Sci. U. S. A.* **113**, E6307–E6315 (2016).

54. R. Sayal, J. M. Dresch, I. Pushel, B. R. Taylor, D. N. Arnosti, Quantitative perturbation-based analysis of gene expression predicts enhancer activity in early Drosophila embryo. *Elife*. **5** (2016).

55. Y. Zhou, X. Liu, E. M. Engstrom, Z. L. Nimchuk, J. L. Pruneda-Paz, P. T. Tarr, A. Yan, S. A. Kay, E. M. Meyerowitz, Control of plant stem cell function by conserved interacting transcriptional regulators. *Nature*. **517**, 377–380 (2015).

56. Y. H. Su, C. Zhou, Y. J. Li, Y. Yu, L. P. Tang, W. J. Zhang, W. J. Yao, R. Huang, T. Laux, X. S. Zhang, Integration of pluripotency pathways regulates stem cell maintenance in the Arabidopsis shoot meristem. *Proc. Natl. Acad. Sci. U. S. A.* **117**, 22561–22571 (2020).

57. M. Kieffer, Y. Stern, H. Cook, E. Clerici, C. Maulbetsch, T. Laux, B. Davies, Analysis of the transcription factor WUSCHEL and its functional homologue in Antirrhinum reveals a potential mechanism for their roles in meristem maintenance. *Plant Cell*. **18**, 560–573 (2006).

58. B. Senay-Aras, W. Chen. Stochastic Cis-elements Binding Model. https://zenodo.org/badge/latestdoi/349283086 (2022).

59. A. Do, MeristemBasic_p. https://zenodo.org/badge/latestdoi/501822165 (2022).

60. A. Do, BasicCisElementAnalyzer. https://zenodo.org/badge/latestdoi/498280124 (2022)

61. M. R. Roussel, R. Zhu, Validation of an algorithm for delay stochastic simulation of transcription and translation in prokaryotic gene expression. *Phys. Biol.* **3**, 274–284 (2006).

62. E. Azpeitia, A. Wagner, Short Residence Times of DNA-Bound Transcription Factors Can Reduce Gene Expression Noise and Increase the Transmission of Information in a Gene Regulation System. *Frontiers in Molecular Biosciences*. **7** (2020).

63. P. S. Gutierrez, D. Monteoliva, L. Diambra, Cooperative binding of transcription factors promotes bimodal gene expression response. *PLoS One*. **7**, e44812 (2012).

64. U. Brand, M. Grünewald, M. Hobe, R. Simon, Regulation of CLV3 expression by two homeobox genes in Arabidopsis. *Plant Physiol.* **129**, 565–575 (2002).

Acknowledgments

We thank Kyle Hill, Vanessa Ceja, Dariush Nejad, Isabel Gutierrez, Valery Franco, and Paul Rubiro for supporting experimental work. Alex Plong for comments on the manuscript. The 3D computational model utilized the simulation framework developed by Dr. Henrik Jonsson (*23*) as its base framework. Additional helpful comments were provided by Niklas Korsbo.

Funding: This work was supported by:
National Science Foundation Grant IOS-2055690 (GVR, WC, Michelle Digman)

RSAP-AES mission funding to (GVR)
National Science Foundation Grant DMS-1762063 through the joint NSF DMS/NIH NIGMS Initiative (MA, GVR, WC)

Author contributions:

Conceived research: KR, GVR, WC
Experimental investigation: KR, AD, MP, GVR
Single cell model and simulation: BSA, WC
3D model and simulation: AD, BSA, WC
Writing—original draft: KR, AD, BSA, WC, GVR
Writing—review & editing: KR, AD, BSA, MP, MA, WC, GVR

Competing interests: Authors declare that they have no competing interests.

Data and materials availability: All data needed to evaluate the conclusions in the paper are present in the paper and/or the Supplementary Materials.

Code availability: 1. An open-source MATLAB/C++ implementation of the computational model of transcription is available at GitHub (https://github.com/weitaoc/SAM.git and https://github.com/Ado012/MeristemBasic_p) or in Zonodo (DOI: 10.5281/zenodo.6632514 and DOI: 10.5281/zenodo.6629834) (*58, 59*) 2. Code for cis-element analysis is available at https://github.com/Ado012/BasicCisElementAnalyzer or in Zonodo (DOI: 105201/zenodo.6632279) (*60*).

Figures and Tables

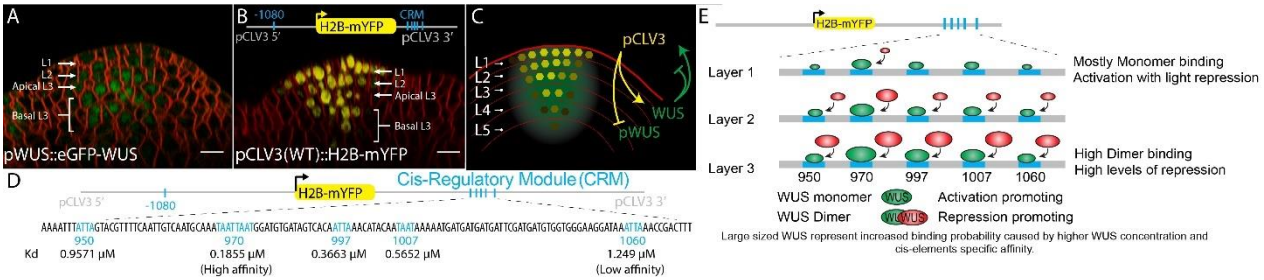

Fig. 1. Cis-Regulatory Module (CRM) required for *CLV3* activation and repression. Side views of wild-type meristems with the WUS protein reporter *pWUS::eGFP-WUS* (**A**) and CLV3 transcriptional reporter containing all five wild-type cis-elements within the 3' CRM *pCLV3(wild-type)::H2B-mYFP* (**B**). Scale bar = 10µm. (**C**) Side view of a SAM cartoon showing WUS protein distribution (green) and CLV3 (yellow) which form a regulatory feedback loop across cell layers. The *CLV3* CRM; a cluster of WUS binding cis-elements, interacts with the WUS concentration to repress and activate *CLV3*. CLV3 signals to WUS at both the post-translation level, enriching the WUS protein, and transcriptional level, repressing *WUS* expression. (**D**) Schematic of the *CLV3* gene including the location and K_d of WUS binding TAAT cis-elements (cyan) of the *CLV3* CRM. (**E**) Schematic of WUS monomer and dimer binding to the *CLV3* cis-elements depending on the WUS concentration gradient (across SAM cell layers) and the relative affinities of cis-elements.

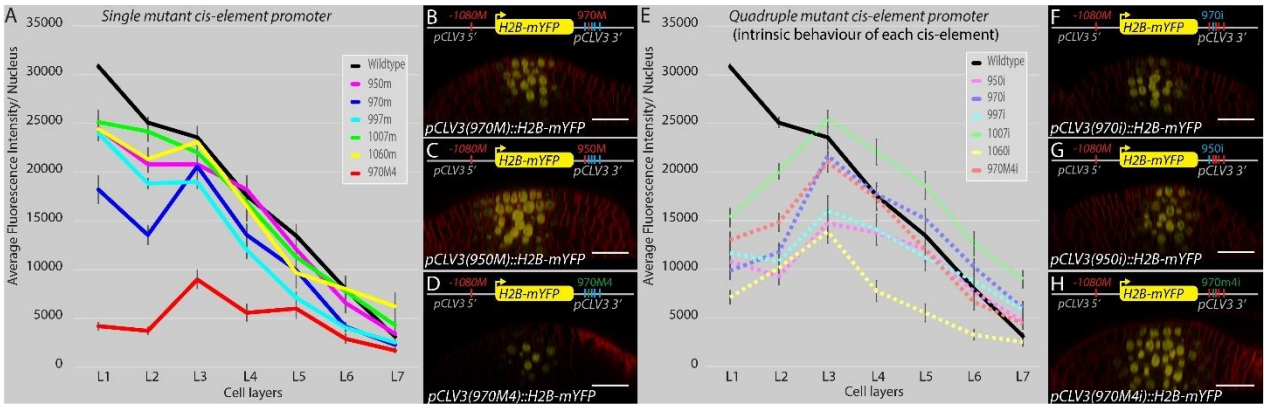

Fig. 2. The number of cis-elements and affinity influence the collective behavior of the CRM in regulating *CLV3* activation and repression. Average fluorescence levels (mean ±S.E.) of H2B-mYFP in different cell layers of various *pCLV3::H2b-mYFP* promoter variants carrying a mutation in single cis-elements of the 3' CRM (**A**). (**B**-**D**) Side views of wild-type meristems showing various mutant *pCLV3::H2B-mYFP* reporter expression patterns. Single cis-element mutants-970M (**B**), -950M (**C**), a higher affinity mutant 970M4 (**D**). Average fluorescence levels (mean ±S.E.) of H2B-mYFP in different cell layers of various *pCLV3::H2b-mYFP* promoter variants carrying mutations in four of the five cis-element mutants [quadruple mutants] (**E**). Side views of wild-type meristems showing various mutant *pCLV3::H2B-mYFP* reporter expression patterns. Quadruple mutant [mutants -950M,997M,1007M,1060M] referred to as 970 intrinsic [970i] (**F**), [mutants- 970M,997M,1007M,1060M] referred to as 950 intrinsic [950i] (**G**), and [mutants -950M,997M,1007M,1060M] referred to as 970-M4 intrinsic [970-M4i] (**H**). All cis-element mutations within the CRM in the 3' region were generated in

the mutant-1080 cis-element background. In all images, scale bar = 20 μm. (**A** and **E**) The error bars represent the standard error. (in all cases, n=4 represents independent transformants).

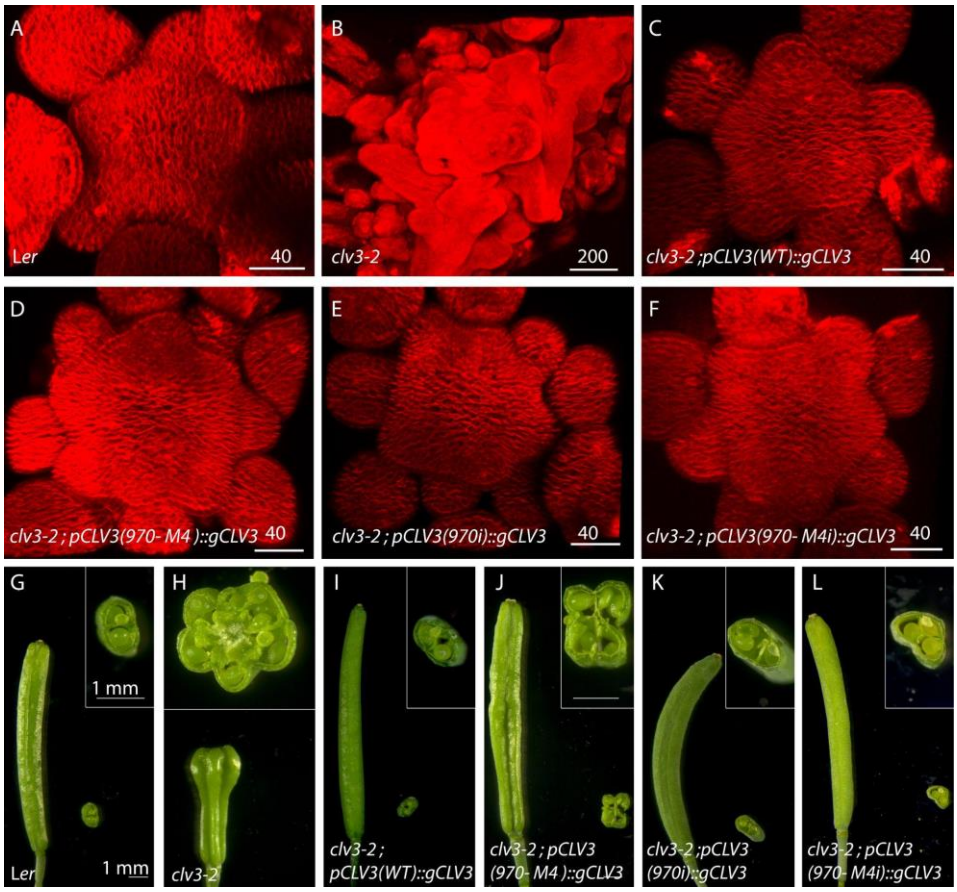

Fig. 3. Functional analysis reveals the importance of the collective behavior of the *CLV3* CRM. (**A-F**) Top views of 3D-reconstructed SAMs stained with plasma membrane dye-FM4-64 (Red). Wild-type (**A**), *clv3-2* (**B**), and *clv3-2* complemented with wild-type genomic *CLV3* (*gCLV3*) expressed from the wild-type *CLV3* promoter [*pCLV3(WT)::gCLV3;clv3-2*] (**C**), *CLV3* promoter carrying high affinity 970M4 cis-element [*pCLV3(970-M4)::gCLV3;clv3-2*] (**D**), CLV3 promoter carrying loss of binding mutation in 950, 997,1007, and 1060 [*pCLV3(970i)::gCLV3;clv3-2*] (**E**), and *CLV3* promoter carrying high-affinity mutation-970-M4 and loss of binding mutations in 950, 997, 1007, and 1060 [*pCLV3(970-M4i)::gCLV3;clv3-2*] (**F**). (**G-L**) Side views of intact siliques and cross section of sliced siliques. Insets show a higher magnification view of the cross section of the sliced siliques. Wild-type (**G**), *clv3-2* (**H**) and [*pCLV3(WT)::gCLV3;clv3-2*] (**I**), [*pCLV3(970-M4)::gCLV3;clv3-2*] (**J**), [*pCLV3(970i)::gCLV3;clv3-2*] (**K**), and [*pCLV3(970-M4i)::gCLV3;clv3-2*] (**L**). Scale bars (in μm) are given on individual panels in **A-F** and the scale bars in **G-L** are 1 mm.

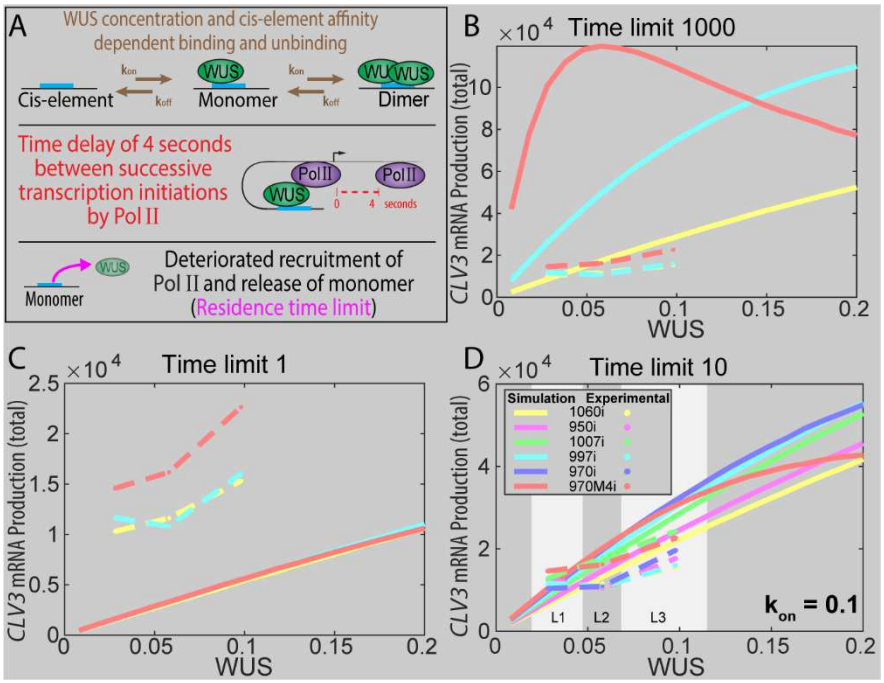

Fig. 4. WUS protein time limit on cis-elements determines the *CLV3* levels and domain of expression. (**A**) WUS concentration dependent binding [k_{on}WUS], k_{on} is the association rate, and cis-element affinity dependent unbinding [$k_{off} = K_d k_{on}$] determine three possible WUS occupancy states: unbound (zero WUS), monomer bound (one WUS), and dimer bound (two WUS). We assume only the monomer bound is able to recruit the RNA Polymerase II (Pol II). A 4 second gap between recruitment of successive Pol II molecules was estimated from the Pol II elongation rate and the size of Pol II footprint on the DNA. Additionally multiple rounds of Pol II recruitment by WUS monomer deteriorate the ability of WUS to recruit additional Pol II (residence time limit). (**B-D**) Single cell model of WUS mediated activation of *CLV3* from single cis-element promoters (four mutated and only one functional cis-element). (**B-D**) Show the scaled simulation results of highest (970M4i), intermediate (997i) and lowest (1060i) affinity cis-elements with the residence time limit of 1000s (similar expression pattern as without the time limit since the time limit is extremely large) (**B**), 1s (**C**) or 10s (**D**). (**D**) Shows all five cis-elements in addition to 970M4i. (**D**) also shows an approximate WUS concentration range to reflect the corresponding WUS fold changes from L1, L2, and L3 layers.

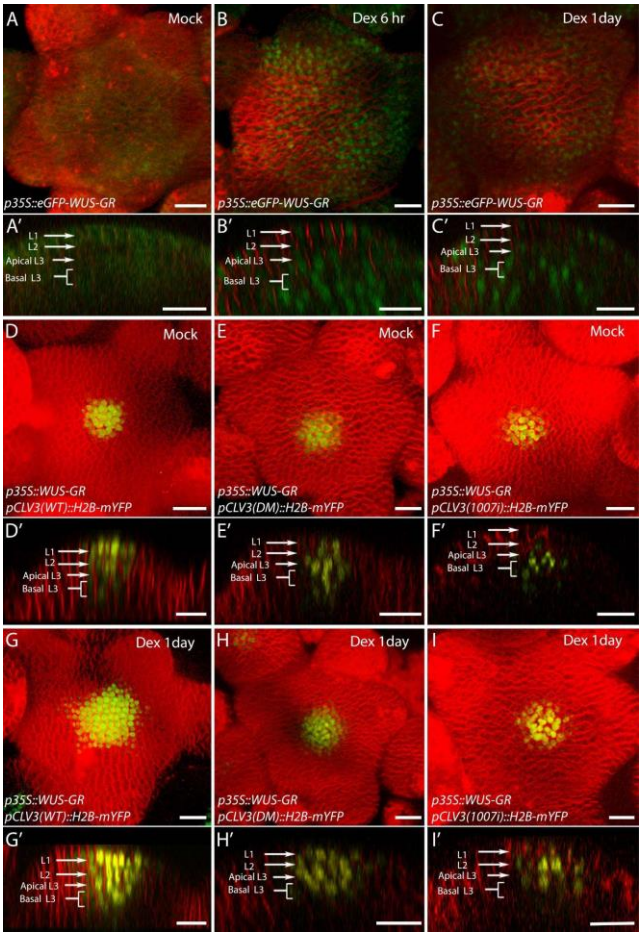

Fig. 5. The number of cis-elements determine the sensitivity of *CLV3* promoter to the dynamic changes in the WUS protein accumulation. (**A-C**) SAMs showing WUS protein accumulation patterns (*p35S::eGFP-WUS-GR*) upon its Dex-induced nuclear translocation at 6 hours (**B**) and at 24 hours (**C**), and upon mock treatment (**A**). (**D-I**) *p35S::WUS-GR* expressing SAMs showing *pCLV3::H2B-mYFP* reporter expression of wild-type *CLV3* promoter (**D**), the double mutant promoter [970 and 997 mutants] (**E**) quadruple mutant promoter [970, 997, 950 and 1060 mutants] (**F**) upon mock treatment. The *pCLV3* reporter expression of the corresponding genotypes after 24 hour Dex treatment is shown in **G-I**. (**A-I**) 3D reconstructed top views of SAMs and corresponding side views shown in **A'-I'**. Plasma membrane stain-FM4-64 (red), eGFP-WUS-GR (green) and H2B-mYFP (yellow). Scale bar = 20 μm.

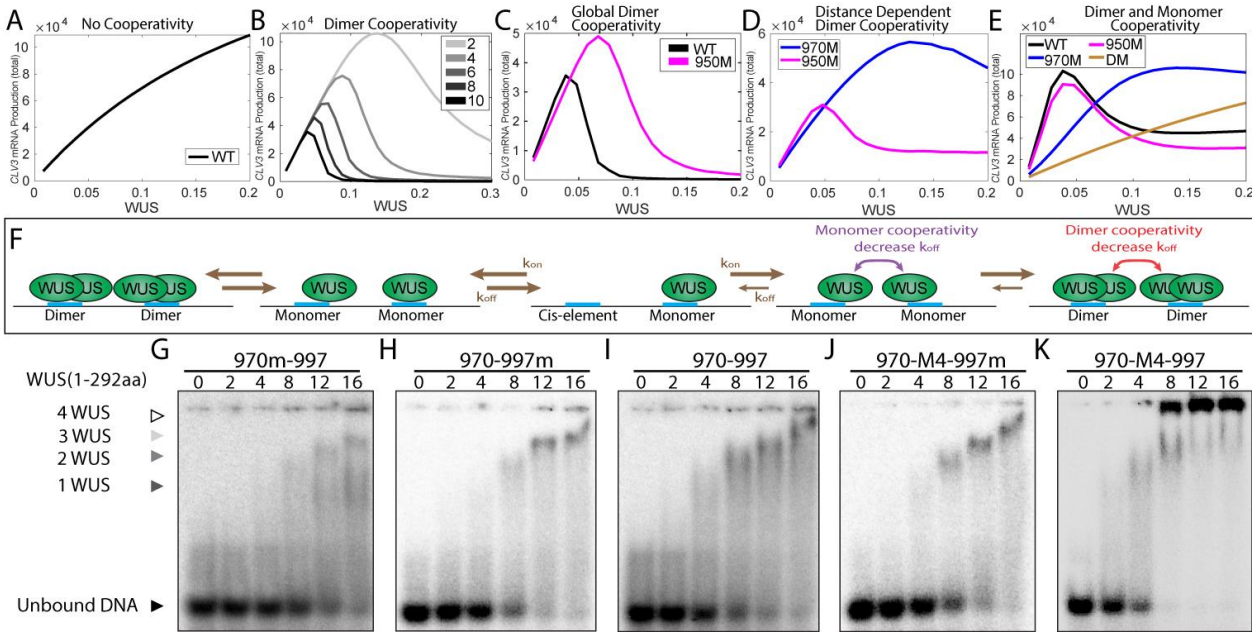

Fig. 6. Cooperativity among cis-elements regulate *CLV3* expression. Average *CLV3* mRNA levels from single cell simulations in response to WUS concentration without cooperativity (**A**), at different strengths of dimer cooperativity (**B**), when dimer cooperativity between every cis-element is considered (**C**), when the dimer cooperativity depends on the intervening distance between cis-elements (**D**), and when both WUS monomer and dimer cooperativity were considered (**E**). (**F**) Binding and unbinding dynamics of WUS monomer and dimer on cis-elements. (**G-K**) Gel shift assay of increasing concentrations of full length WUS (1-292aa) to probes of similar length that cover the 970 and 997 cis-elements. Probes with loss of binding mutations to the TAAT elements in the 970 cis-element (**G**) and the 997 cis-element (**H**). (**I**) Probe with wild-type copies of the 970 and the 997 cis-elements. Probes that contain higher affinity mutant 970-M4 along with the mutant 997 (**J**) or the wild-type 997 cis-element (**K**). (**G-K**) Arrowheads denote higher order WUS complexes; monomer (dark grey), dimer (light grey), and higher complexes (white). The unbound probe (black).

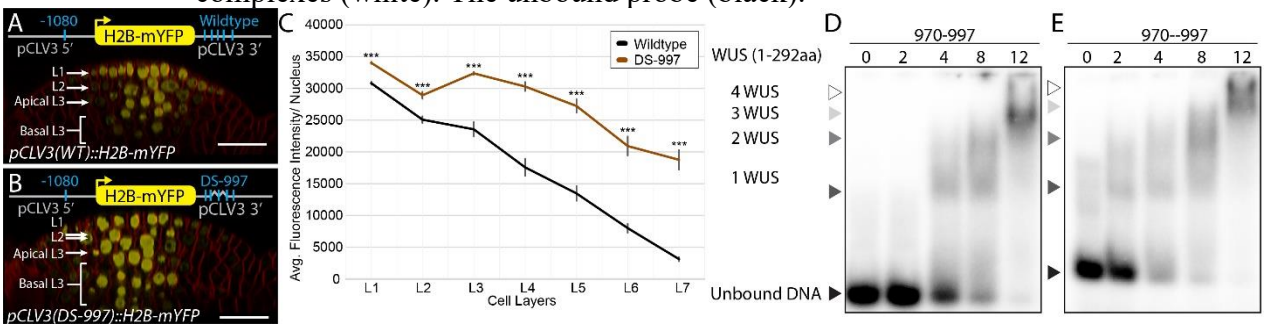

Fig. 7. Spacing between cis-elements is critical for *CLV3* repression. Side view of SAM showing the wild-type *pCLV3::H2B-mYFP* expression (**A**) and mutant *CLV3* reporter containing duplicated sequence to the left (5') and right (3') of the 997 cis-element [Double sequence around 997- DS997] (**B**). (**C**) Average H2B-mYFP fluorescence intensity (mean ±S.E.) in 10 centrally located nuclei/cell layers quantified from four independent transformants of wild-type and DS-997 [n =4] *** p <0.001. EMSAs showing increasing concentrations of full length WUS (1-292 aa) WUS bound to the probe containing the 970 and 997 cis-elements with wild-type intervening sequence (**D**) or a duplicated intervening sequence (**E**).

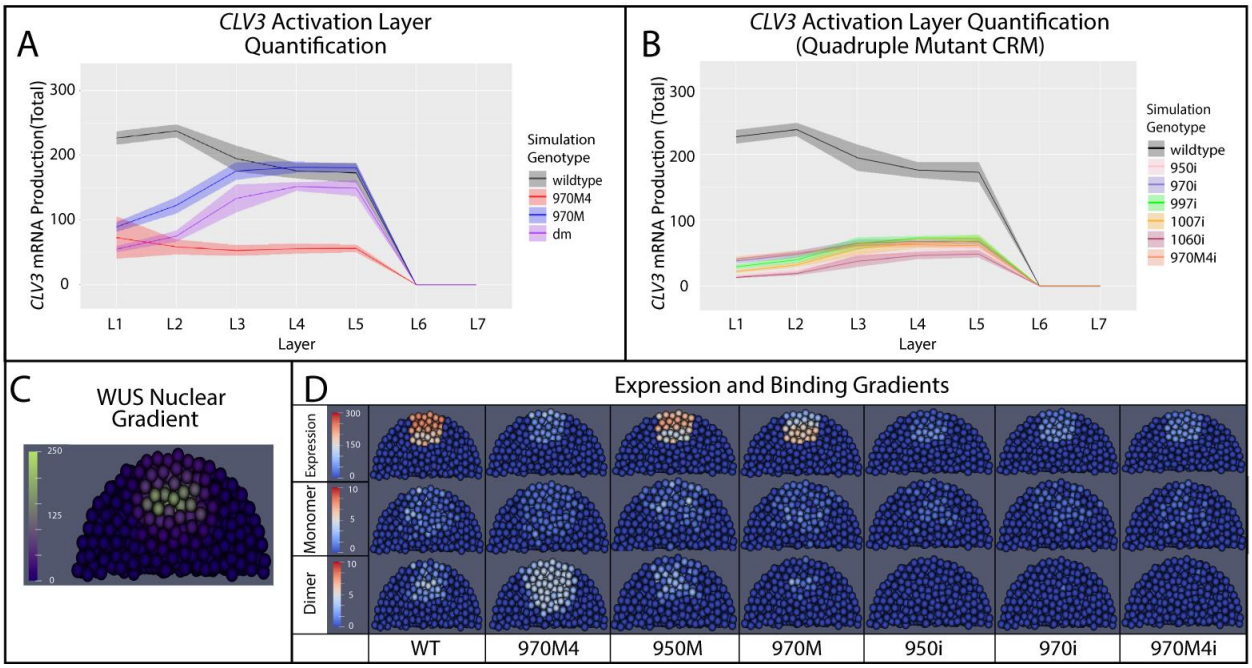

Fig. 8. Simulated *CLV3* dynamics and WUS protein complexes in the 3D SAM model. (**A**) Levels of *CLV3* (mean = line, SD = shaded area) activation in wild-type system and system with selected mutated cis-elements. (**B**) Levels of *CLV3* gene activation (mean = line, SD = shaded area) in wild-type system and system carrying all possible combinations of quadruple mutants (reflects intrinsic behavior of each functional cis-element). Line indicates mean *CLV3* in different cell layers. Shaded area indicates standard deviation of activation among the cells in a given cell layer. L1-L7 indicates the layers of the SAM from outermost CZ to inner layers of the RM. (**C**) Spatial distribution of nuclear localized WUS. (**D**) Median longitudinal sections of simulated SAMs showing WUS monomer (center panel), WUS dimer (bottom panel) and *CLV3* expression (top panel) in wild-type and system carrying various mutant cis-elements-970M4, 950M, 970M, 950i, 970i and 970M4i.

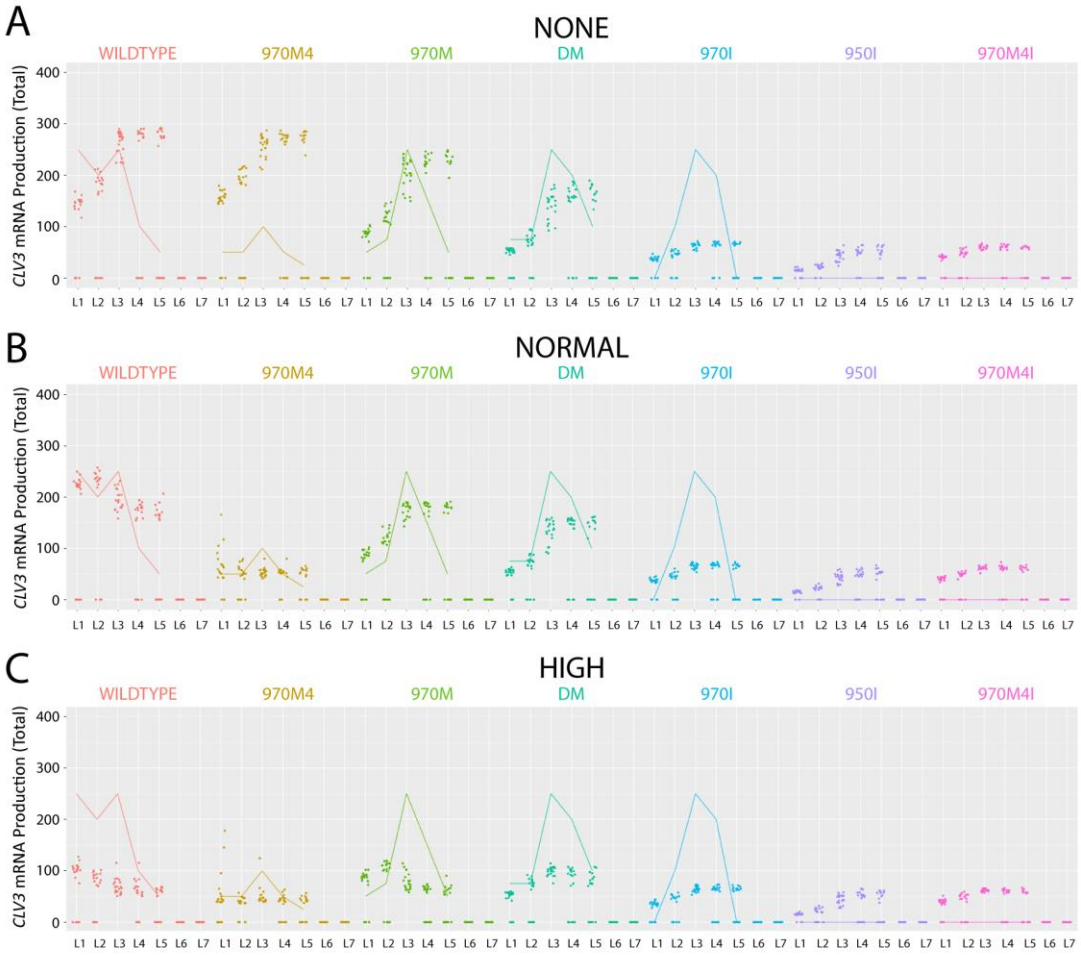

Fig. 9. Cooperativity levels influence *CLV3* activation. *CLV3* activation level of wild-type *CLV3* CRM and mutant *CLV3* CRMs under various cooperativity levels. (**A**) No cooperativity; simulations had no cooperativity between cis-elements. (**B**) Normal cooperativity: Normal cooperativity values (0.01 Monomer Cooperativity, 0.2 Dimer Cooperativity) used in the default simulations. (**C**) High Cooperativity: Simulations with 10x the cooperativity of the default values in the simulation i.e. (0.001 Monomer Cooperativity, 0.02 Dimer Cooperativity). Dots are simulation values for a cell. Lines are corresponding average expression values from experimental studies. Colors represent different mutants.

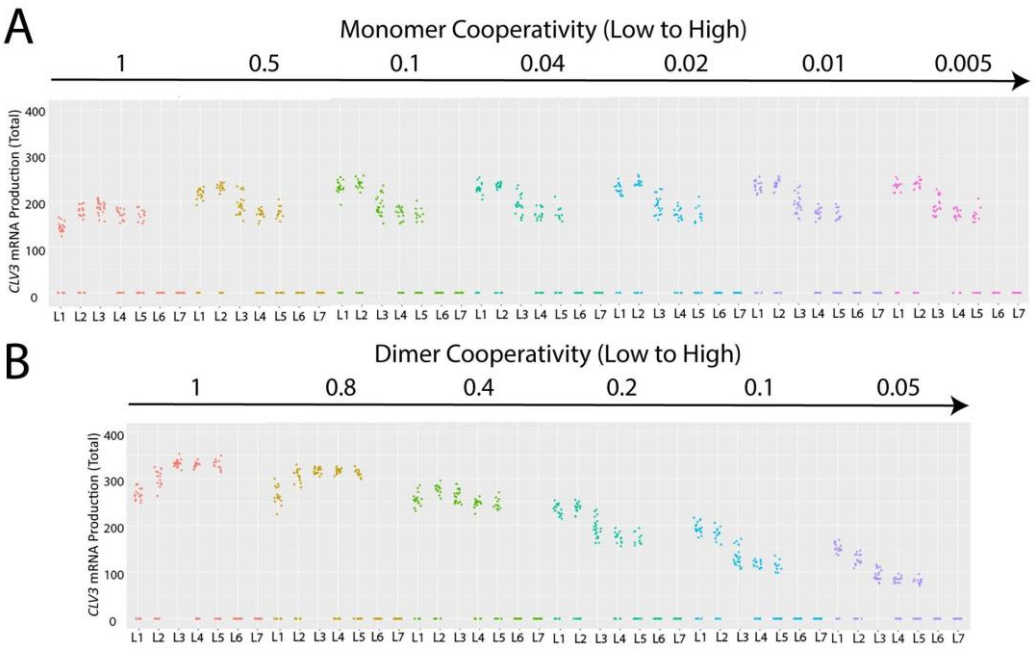

Fig. 10. Independent perturbations of the monomer or dimer cooperativity. The effect of changes in monomer cooperativity (from 1 to 0.005) and dimer cooperativity (from 1 to 0.05) on *CLV3* activation. The direction of the arrows indicate an increase in cooperativity. In row (**A**) dimer cooperativity was held constant at 0.2 while monomer cooperativity was varied (1 - 0.005). In row (**B**) monomer cooperativity was held at 0.01 and dimer cooperativity was varied (1 - 0.05). A complete table of changes in monomer and dimer cooperativity is presented in Fig. S6. The individual graphs represent the *CLV3* activation in different cell layers (L1 to L7) of simulated SAMs under the cooperativity levels noted for each simulation. The dots represent the values of the *CLV3* signal for individual simulated cells.

ScienceAdvances
AAAS

Supplementary Materials for

• Concentration-dependent transcriptional switching through a collective action of cis-elements

Kevin Rodriguez, Albert Do, Betul Senay-Aras, Mariano Perales, Mark Alber, Weitao Chen*, G. Venugopala Reddy*

*Corresponding authors. Email: weitaoc@ucr.edu or venug@ucr.edu

This PDF file includes:

Supplementary Text
Figs. S1 to S11
Tables S1 to S7

Other Supplementary Materials for this manuscript include the following:

Data S1

Supplementary Text

Plant growth conditions and genotypes.

All plants were grown at 25ºC under continuous light. All transgenic plants were generated in the Landsberg *erecta* background. The wild-type p*CLV3::H2B-mYFP* reporter has been described earlier (*24*). Various cis-element mutant p*CLV3::H2B-mYFP* reporters described were generated through PCR mutagenesis by using appropriate primers listed in Table S4. The sequence of the *pCLV3::H2B-mYFP* and *pCLV3::CLV3genomics* are included in Data S1, while the mutant CRM excerpts are included in Table S5. The p*35S::eGFP-WUS-GR* transgenic plants described in the earlier study (*53*) were crossed to the wild-type p*CLV3::H2B-mYFP*, p*CLV3 (DM)::H2B-mYFP* and p*CLV3 (QM)::H2B-mYFP* reporters (*24*). The progeny was exposed to mock or 10μM Dexamethasone (Dex) for 24 hours and imaged as described below.

Sample preparation and confocal microscopy.

The images were acquired from three-week-old plants. All surrounding older flowers were removed carefully. The excised stem containing the shoot apex was transplanted into a plastic imaging box containing a 1 cm thick layer of 1.5 % agarose. The stem was stabilized by pouring additional amounts of molten agarose, then submerged in deionized water and further processed under a stereomicroscope. The remaining older floral buds covering the SAM were further trimmed with tweezers to expose the SAM. The water was discarded and a droplet of 3% FM-4-64 dissolved in deionized water containing 0.016% silwet-77 was applied to each SAM. After 10 minutes of FM4-64 staining, the plants were submerged in deionized water and imaged by using the Zeiss880 confocal microscope.

Image quantification and analysis

The p*CLV3::H2B-mYFP* reporter expression and *pWUS::eGFP-WUS* nuclear protein accumulation were quantified from four independent SAMs. The mean nuclear fluorescence signal from the ten central most cells in each cell layer were manually selected using a circle tool within the ZEN 2.3 blue edition software. To evaluate the statistical significance, two-tailed t-tests were applied comparing wild-type *CLV3* reporter levels in each cell layer to various mutant reporters described. The quantification of SAM height was carried out as described in (*24*). Two samples on each independent line, for a minimum of nine independent transgenic lines, for each WUS binding cis-element promoter were analyzed. The height was determined from the junction of the 5th primordia to the SAM apex. The carpel number was performed on two samples on each independent line, for a minimum of 5 independent transgenic lines. The multiple comparison was performed by one-way ANOVA followed by Tukey's HSD test using R (v3.6.1) package.

Gel shift assays - EMSA

The purification of wild-type WUS protein (amino acids 1-292) was carried out as described previously in (*24*). His-WUS protein, cloned into pET28α plasmid (Novagen), was expressed in BL21 cells. WUS protein was purified from the soluble lysate using a His-tag protocol (Ni-NTA His-Bind Resins; Novagen) and dialyzed in 20 mM Hepes at pH 7.8 and 100 mM KCl. The EMSA was carried out as described in an earlier study (*23, 24*). Oligonucleotides were radiolabeled with (ϒ-32P) ATP by T4 polynucleotide kinase (NEB) and annealed with complementary oligonucleotides to make double stranded DNA. The protein-DNA binding reaction was performed in a 20 μL reaction mixture: 10fmol probe, 1x binding buffer (20mM HEPES-KOH at pH7.8, 100mM KCl, 1mMEDTA, 0.1% BSA, 200 ng DNA salmon sperm, and 10% glycerol) and His-WUS protein. After a 20 min incubation at RT, samples were loaded into a 6% native polyacrylamide gel. Electrophoresis was performed at 10V/cm for 90 min in 0.5x Tris-borate buffer. Gels were autoradiographed using phospho imaging and Typhon system. The single cis-element probes were same as those used in earlier study (*24*). The sequences of new

oligonucleotide probes containing two cis-elements, the corresponding mutant forms, and probes with altered intervening distance have been listed in Table S2.

BiFC analysis

For the BiFC analyses, the N-terminal fragment of eGFP (NeGFP) from nucleotides 1-465 (AA 1-155), and the C-terminal fragment of eGFP from nucleotides 466-723 (AA 156-241) were generated through an inverse PCR using 5' Phosphorylated oligos in (Table S4) on the PCR4 cloning vector with eGFP-WUS described in (*23*). For generating stable transgenic lines, these constructs were introduced into the *WUS promoter* described in earlier study (*23*). Fifteen independent transgenic plants for each construct were isolated and crossed to each other. The F1 progeny were used for visualizing BiFC signal in SAM tissue.

Description of stochastic single-cell model

In the stochastic single-cell model, the WUS concentration-dependent activation and repression of *CLV3* transcription is modeled as follows. WUS can bind as a monomer or dimer to each of the five cis-elements at different affinities. In particular, it is assumed that only monomers can recruit Pol II for transcription of *CLV3* and one molecule of *CLV3 mRNA* is generated for each Pol II recruitment. The total amount of *CLV3 mRNA* produced is quantified. Specifically, the following five possible stochastic events are considered, where S represents a binding site, P denotes one WUS molecule, SP denotes the WUS monomer bound cis-element, SP_2 denotes a WUS dimer bound cis-element, TSS is the transcription starting site, $Pol\ II$ is RNA Polymerase and $mRNA$ denotes *CLV3 mRNA*:

$S + P \xrightarrow{k_{on}^{M}} SP$ binding with one WUS molecule (WUS monomer) [1]

$SP \xrightarrow{k_{off}^{M}} S + P$ unbinding of WUS monomer creates unoccupied cis-element [2]

$SP + P \xrightarrow{k_{on}^{D}} SP_2$ binding of the second WUS molecule to the WUS monomer (WUS dimer) [3]

$SP_2 \xrightarrow{k_{off}^{D}} SP + P$ unbinding of the second WUS molecule generates WUS monomer [4]

$TSS + SP + Pol\ II \xrightarrow{k_p} TSS(t_1) + SP + Pol\ II(t_2) + mRNA(t_2)$
Recruitment of Pol II by a WUS monomer bound to a cis-element to produce *CLV3* mRNA [5]

In EQ (1) and (2), a single WUS molecule binds an empty cis-element at a rate k_{on}^{M} $(\mu M^{-1}s^{-1})$ and the monomer dissociates at a rate $k_{off}^{M}(s^{-1})$. Similarly in EQ (3) and (4), a second WUS molecule binds a WUS monomer at a rate k_{on}^{D} $(\mu M^{-1}s^{-1})$ and a dimer dissociates at a rate $k_{of}^{D}(s^{-1})$. EQ.5 represents the recruitment of Pol II by a WUS monomer bound to a cis-element, SP, at TSS for *CLV3* mRNA transcription. Pol II molecules are recruited to Transcription Start Site (TSS) at a rate $k_p(s^{-1})$ by any WUS monomer present in CRM. There is a time delay for the release of TSS, Pol II and mRNA. TSS is released with a delay t_1, Pol II and mRNA is released with a delay t_2. We apply the Gillespie algorithm, developed originally to simulate discrete interactions in chemical reaction systems, through the use of Monte Carlo method in determining time step sizes and occurring events. By applying this algorithm, possible events and their associated probabilities are updated in each iteration according to the current status of the cis-elements. In particular, the delayed stochastic simulation algorithm (SSA) (*61*) was applied based on the estimated 4 sec time delay (denoted by $t_1 = t_{delay}$ in the algorithm), involved in the recruitment of successive Pol II molecules to the transcription start site. Assuming $k_{on}^{M} = k_{on}^{D} = k_{on}$ for all sites, the association and dissociation probabilities of monomers are given by (*62*):

$$p_a = \frac{k_{on}}{VN_A} N_P N_S \quad [6]$$

$$p_d = k_{off} N_{SP} \quad [7]$$

where V is the reaction volume, N_A is the Avogadro's number, N_P, N_S and N_{SP} are the number of WUS molecules, cis-elements and WUS monomer bound cis-elements respectively. We consider WUS binding and unbinding events to each cis-element as a separate event and therefore $N_s = N_{SP} = 1$ (or 0 depending on the state of cis-elements in the CRM). Also $\frac{N_P}{VN_A} = [WUS]$ where $[WUS]$ is the concentration of WUS proteins. In the thermodynamic equilibrium, we have $K_d = \frac{k_{off}}{k_{on}}$, where K_d is the affinity of the cis-element and it is determined by EMSA (*24*). Combining these we obtain:

$$p_a = k_{on}[WUS] \quad [8]$$

$$p_d = k_{off} = k_{on} K_d \quad [9]$$

Considering k_{on} as a free parameter, we can conclude that binding propensities depend on WUS concentration and unbinding propensities of WUS monomers depend on affinities of cis-elements. WUS dimers are also modeled similarly by estimating K_d for dimerization according to EMSA data.

Additional assumptions

- WUS concentration is assumed to be constant in time since each binding or unbinding event is not expected to change the overall WUS concentration in the nucleus.
- Dimers are formed in two steps, i.e., first one WUS molecule binds as a monomer and then it becomes dimer if the second WUS molecule binds, as shown in EMSA experiments (*24*).
- If a WUS monomer does not cooperate with other WUS monomers to stabilize each other, it dissociates upon reaching the "residence time limit (RTL)" as explained in the main text. This dissociation of WUS monomers is not directly related to affinities of the cis-elements when only a single cis-element is functional.
- WUS monomers bound to the cis-elements recruit Pol II for transcribing *CLV3* and each Pol II recruitment generates one *CLV3* mRNA. Successive recruitment of Pol II to the transcription start site (TSS) is assumed to happen with an estimated 4 sec time delay. The time delay ($t_1 = t_{delay}$) is based on an 80 bp footprint of Pol II containing protein complex and mRNA elongation rate, which is estimated to be 1.2 kb/min (*37*) $[80bp \times (60\ sec/1200\ bp) = 4\ sec]$. Pol II and *CLV3* mRNA are released with a delay of t_2 seconds upon completion of the transcription, but we assume Pol II is abundant in the system so the total number is unaffected. Since we track the total number of *CLV3* mRNA generated at steady-state, we neglect the second time delay t_2.
- Right after the recruitment of one Pol II by a WUS monomer, the WUS monomer can unbind the cis-element or a second WUS monomer can bind to generate WUS dimer on the same cis-element without affecting transcribing by Pol II.
- Degradation of *CLV3* mRNA is neglected. We tested single cis-element simulations with different degradation values. When degradation rate is high compared to the binding and unbinding rates of WUS molecules, the simulations failed to capture the single cis-element *CLV3* expression behavior observed in the experiments. When degradation is much smaller than binding and unbinding rates of WUS molecules, the simulations could capture the experimental data qualitatively and moreover, the degradation level did not affect the *CLV3* expression pattern qualitatively. Therefore, for simplicity we neglected the degradation of *CLV3* mRNA.

At any given time, the next event can be one of the five stochastic events described in Eq. (1-5), the release of Pol II from TSS (at the end of $t_{delay} = 4s$), or the release of a WUS monomer

with no cooperativity upon reaching the "residence time limit". The remaining time for the release of Pol II from the TSS, the minimum of the remaining times for the release of the monomers bound to cis-elements upon reaching the residence time limit and the waiting period for the next stochastic event are denoted by t_{rem}^1, t_{rem}^2 and τ respectively.

Algorithm

1. Set $t = 0$, the amount of *CLV3* mRNA is zero and TSS and *CLV3* CRM are unoccupied.
2. Propensity functions are calculated for each possible event based on current binding status, denoted by $a_i(t)$ for each event. The sum is denoted by $a_0(t) = \sum_{i=1}^{N} a_i(t)$.
3. Two random numbers r_1 and r_2 are generated from a standard uniform distribution.
4. The waiting time for the next event is calculated as $\tau = -ln(r_1)/a_0$; the next event with the index j satisfying $\sum_{i=1}^{j-1} a_i(t) \leq a_0 r_2 < \sum_{i=1}^{j} a_i(t)$ is chosen.
5. Compare τ with t_{rem}^1 and t_{rem}^2. Apply one of a, b or c below:
    a. If *CLV3* CRM is bound with a WUS monomer with no cooperativity and (($t_{rem}^1 < min(\tau, t_{rem}^2)$ or ($t_{rem}^1 < \tau$ and TSS is unoccupied)): Update the time as $t \leftarrow t + t_{rem}^1$ and update *CLV3* CRM by unbinding the WUS monomer, set $t_{rem}^1 = 0$ and if TSS is occupied, update $t_{rem}^2 = t_{rem}^2 - t_{rem}^1$.
    b. If Pol II is bound to TSS and ($t_{rem}^2 < min(\tau, t_{rem}^1)$ or ($t_{rem}^2 < \tau$ and *CLV3* CRM is not bound to a WUS monomer with no cooperativity)): Update the time as $t \leftarrow t + t_{rem}^2$, increase the amount of *CLV3* mRNA by 1, set $t_{rem}^2 = 0$ and set TSS to be unoccupied. If at least one WUS monomer with zero cooperativity is bound, update $t_{rem}^1 = t_{rem}^1 - t_{rem}^2$.
    c. If ($\tau < min(t_{rem}^1, t_{rem}^2)$) or (TSS is unoccupied and $\tau < t_{rem}^1$) or (*CLV3* CRM is not bound to a WUS monomer with no cooperativity and $\tau < t_{rem}^2$) or (TSS is unoccupied and *CLV3* CRM is not bound to a WUS monomer with no cooperativity): Update the time as $t \leftarrow t + \tau$ and update the current state of the *CLV3* CRM or TSS according to the selected event j. If TSS is occupied, update $t_{rem}^2 = t_{rem}^2 - \tau$. If at least one WUS monomer with zero cooperativity is bound, update $t_{rem}^1 = t_{rem}^1 - \tau$. If the selected event is Pol II recruitment, set $t_{rem}^2 = t_{delay}$. If the selected event is a WUS monomer binding without cooperativity, set $t_{rem}^1 = RTL$.
6. If $t < t_{final}$, go to Step 2, otherwise stop.

For each stochastic simulation, the activation of *CLV3* is obtained by calculating the total amount of mRNA accumulated during the simulation period. The mean value from a sufficiently large number of independent simulations (*41*) was generated and compared with the experimentally quantified *CLV3* expression measured by fluorescence quantification of *pCLV3::H2B-mYFP* (Fig. 2). In Fig. 4, 6A-E and Fig. S5, $t_{final} = 1.6 \times 10^6$ in the simulations, and in Fig. S9, $t_{final} = 1.6 \times 10^5$.

Parameters

The K_d values for events EQ.1 and EQ.2, which are binding and unbinding events of a WUS monomer to different cis-elements, are represented by $K_d = k_{off}^M / k_{on}^M$ and they are determined by the EMSA experiments (*24*). With these K_d values (Table S1), first we simulated WUS monomer binding and unbinding and compared the simulation results with the quantitative data from EMSA experiments with WUS that lacked the C-terminal homodimerization domain. In these simulations, we chose k_{on} values between 0.1 and 1 which fit well to the experimental data (Fig. S4A). Next, we simulated monomer and dimer binding and unbinding similar to the EMSA experiments with WUS that had the C-terminal homodimerization domain. Since the quantitative

data for WUS dimerization (K_d values) is not available, we matched EMSA data qualitatively as follows. We simply considered K_d^d, the dimerization K_d, the same as monomer K_d and we chose $k_{on}^M = k_{on}^D = 0.1$. We tested this assumption by simulating the single cis-element EMSA experiments with WUS that had the C-terminal homodimerization domain. Since the quantification of the proportions of monomers and dimers in these experiments is not possible, we compared our simulations to the EMSA experiments qualitatively. For the cis-elements 970i, 970M4i, 997i and 1007i, the assumption $K_d^d = K_d$ could generate results similar to the data qualitatively, so we proceeded with this assumption for these cis-elements. But for the low affinity cis-elements 950i and 1060i, the assumption that $K_d^d = 0.5K_d$ gave better results. In summary, we defined $k_{off}^M = K_d \cdot k_{on}$ and $k_{off}^D = K_d^d \cdot k_{on}$ with $k_{on} = 0.1$ (Fig. S4B). In EQ5, k_p is a free parameter that was tested to ascertain how varying k_{on} and k_p affects intrinsic activation of *CLV3* in the case of highest (970M4i) and lowest affinity (1060i) cis-elements (Fig. S9). The total amount of transcriptional output increased as k_p increased from 0.2 to 100 for fixed k_{on}. To calibrate k_{on} and k_p values, we simulated our model for highest affinity single cis-element 970M4i and lowest affinity single cis-element 1060i, and calculated the ratio of the experimental *CLV3* reporter values for 970M4i and 1060i in different cell layers. For small k_{on} values like k_{on}=1 or smaller, we see a huge difference between simulations and experimental data. For larger values such as k_{on}=10 and k_p=10, the ratio of expressions of 970M4i and 1060i gets closer to experimental measurements (Fig. S11A). However, for multiple cis-element behavior with k_{on}=10 and k_p=10 (WT, 970M, 950M and DM [970M-997M]), we observed high levels of expression at low WUS concentrations for all mutants including 970M and DM, similar to the wild-type, which is contrary to the experiments. We also tried simulations under different cooperativity assumptions and levels and obtained similar results that didn't match the experiments (Fig. S11B-D). Therefore, although it is possible to generate the single cis-element behavior using larger values of k_{on} and k_p, the multiple cis-element behavior could not be generated. In contrast, using smaller values of k_{on} and k_p coupled with the monomer residence time limit, the model was able to generate both single and multiple cis-element behaviors consistent with experiments. Therefore, k_p=0.2 and k_{on}=0.1 are used in all simulations of the single cell model.

The WUS levels in different cell layers in the single cell model were chosen to satisfy the experimental quantification where WUS concentration decreases by ~1.5 fold from L2 to L1 and ~2 fold from L3 to L2 (*51*). The chosen WUS levels were able to generate the experimentally observed *CLV3* expression.

Cooperativity

The free energy of binding of a WUS molecule to a cis-element can also be affected by the interaction between WUS bound to other cis-elements in the CRM. This interaction between WUS molecules might increase the binding propensity of the new WUS molecules or stabilize the bound ones, e.g. decrease the unbinding propensity of the bound WUS molecules (*63*), which was modeled as cooperativity. We first considered equal cooperativity between every two cis-elements in the model, which couldn't generate consistent results as the experimental data (Fig. 6C). Cooperativity as a function of the distance between binding sites, d, was studied before (*54*). To model the strength of the interaction between WUS molecules bound to different cis-elements, we defined a function $f(d)$ which decreases as d increases. To model the increase in the binding propensity due to cooperativity we multiplied the original propensity with $f(d)$ and to model the decrease in unbinding propensity we divided that with $f(d)$. A linear function did not give rise to biologically consistent behavior, therefore we considered the following nonlinear function: $f(d) = -a_d \, arctan\,(a_c(d - b_d)) + 1.5708\, a_d + 1$ to reduce the difference between wild-type and 950M on *CLV3* expression pattern. If $a_i(t) = k_{on} WUS$ is the propensity function for binding

of a TF to a cis-element when there is no interaction, the binding propensity becomes $a_i(t) = k_{on}WUS(\Pi_{j=1}^{n-1} f(d_j))$ where d_j is the distance between any two cis-elements and n is the number of functional cis-elements that are bound with WUS monomers (or dimers). We chose this function in order to reproduce the experimental observations for simplicity. The function f constructed in this way satisfies that: if the distance between two cis-elements is less than a threshold value, then f takes some value much greater than 1, representing the cooperativity is strong; if the distance between two cis-elements is greater than another threshold value, then $f(d)$ becomes close or equal to 1, which means a decreased or zero cooperativity; if the distance is between these two threshold values, then $f(d)$ decreases as the distance increases. Similarly, the unbinding propensity of a TF molecule is $a_i(t) = k_{off}$ when there is no interaction between bound molecules and it becomes $a_i(t) = k_{off}/(\Pi_{j=1}^{n-1} f(d_j))$ when there is some interaction. In summary, the cooperativity between cis-elements increases binding probability and also decreases unbinding probability of WUS molecules. The parameters for the cooperativity was determined by comparing the *CLV3* expression obtained in simulations to the experimentally observed *CLV3* expression patterns of various cis-element mutants. The model description of cooperativity used to generate results presented in Fig. 6 is provided below.

Fig. 6A: No cooperativity between cis-elements is considered. Unbinding propensity $a_i(t) = k_{off}$ stays the same.

Fig. 6B, C: WUS dimer cooperativity is included, which is equal between every cis-element independent of the intervening distance. Unbinding propensity becomes $a_i(t) = k_{off}/(a_d + 1)^{n-1}$ where n is the number of functional cis-elements that are bound with dimers and a_d is a constant. $a_d = 2,4,6,8,10$ are tested for the simulation results presented in the Fig 6B.

Fig. 6D: Distance dependent WUS dimer cooperativity is considered. Unbinding propensity becomes $a_i(t) = k_{off}/(\Pi_{j=1}^{n-1} f(d_j))$. $a_d = 40$ and $b_d = 40$ in these simulations.

Fig. 6E: Distance dependent WUS monomer and dimer cooperativity is considered. Binding propensity becomes $a_i(t) = k_{on}WUS(\Pi_{j=1}^{n-1} f(d_j))$ and unbinding propensity becomes $a_i(t) = k_{off}/(\Pi_{j=1}^{n-1} f(d_j))$. The parameters for these simulations are given in Table S2.

Description of 3D cell-based model

We model the SAM by a half dome shape consisting of more than 1000 unit spheres representing individual cells (*23*). The simulated SAM is divided into multiple layers. The first layer of cells represents Layer 1 (L1) and it includes all cells with centers higher than 8.5 units above the center of the base of the SAM. The next layer of cells represents Layer 2 (L2) and includes all cells with centers between 8-8.5 units above the base center of the SAM. Below this the layers are defined as follows: L3: 8-6.5 units, L4: 7 and 6 units, L5: 6 and 5 units, L6: 5 and 4 units, and L7: 4 and 3 units. Production of *CLV3* mRNA is limited to a cylinder shaped spatial domain and the radius of the cylinder is given in Table S3. Since in each cell there exists two copies of CRMs, we consider two independent identical groups of 5 cis-elements in the model. Each simulation is run sufficiently long to achieve the steady-state behavior. The 3D cell-based model follows the same approach as the stochastic single-cell model for individual cells, except the following modeling assumptions:

1. WUS gradient at the tissue level. A gradient of nuclear WUS proteins is chosen to be consistent with the experimental quantifications across different layers and is fixed throughout simulations under different mutant cis-elements conditions. The local concentration of WUS is

then used in the stochastic binding model inside each cell to obtain the *CLV3* expression pattern in the tissue.

2. Stochastic binding dynamics in individual cells. The stochastic single-cell model is applied for each CRM inside individual cells with some minor modifications described as below:

i. For all binding events, the propensity of binding becomes $k_{on}\ WusConc/WusSat$ instead of $k_{on}\ WusConc$ used in the stochastic single-cell model. This is because WUS concentrations used in the cell-based model have a different scale from the one in the single-cell model.

ii. For the monomer cooperativity, it is assumed that 970 plays a dominant role due to its higher affinity. In particular, the propensity function for monomer unbinding events associated with 970 is $k_{on}K_d c_{coop}^{n+n_{970}}$, where n is the number of WUS monomers bound to all other cis-elements and n_{970} is a constant calibrated in the model (Table S3). For all other cis-elements, the propensity function for monomer unbinding events becomes $k_{on}K_d c_{coop}^{n}$, where n is the number of WUS monomers bound to 970 and $c_{coop} = monomerCoopt$ is a parameter calibrated in the model (Table S3, Fig. 9-10).

Regarding the dimer cooperativity, for all five cis-element, the propensity function for dimer unbinding events is $k_{on}K_d c_{coop}^{n}$, where n is the number of WUS dimers bound to neighboring nonempty cis-elements. For 970M4, due to its enhanced affinity, the propensity function for dimer unbinding event is $k_{on}K_d c_{coop}^{n+n_{970}}$, where n is the number of WUS dimers bound to all other cis-elements and $c_{coop} = dimerCoopt$ is a parameter calibrated in the model (Table S3, Fig. 9-10).

The cooperativity modeled in this way is similar to the one used in the single-cell model which has a threshold such that the cooperativity associated with the closest (or adjacent) unoccupied neighbors is much stronger.

3. Parameters. This 3D cell-based model involves multiple parameters which can't be estimated directly from experimental data. In particular, those involved in the stochastic binding dynamics in each cell are calibrated using the stochastic single-cell model and the same values are adopted. Parameters that are involved in the 3D cell-based model only are provided in Table S3.

Bioinformatic analysis of Cis-element clusters in WUSCHEL regulated genes

To search for the occurrence of cis-element clusters in WUS regulated genes, a list of genes that were upregulated and downregulated by WUS (*27*) in the presence of protein synthesis inhibitor Cyclohexamide were considered. The search begins with the main function Arabmotifsearch(). A target file containing the WUS regulated genes, a GFF file containing annotation information, and the TAIR10 sequence are input along with the desired names of the output files. The annotation file is broken into several pieces including chromosome, gene names, and start and end positions.

For each gene target, the function targetScanner() is run, associating the target gene with a chromosome and sequence. The function MotifPrelimScanner() scans the sequence defined from 3000 bp before the gene start (Transcription start site) to 3000 bp after the gene end (Transcription stop site) for TAAT/ATTA cis-elements. The cis-elements list is fed into ClusterScanner() to detect cis-element clusters/CRMs which are defined as strings of at least 4 cis-elements which are within 50 bp of the previous one.

Each CRM is then scanned for complex cis-elements in Complexcorescanner() which is defined as a string of cis-elements where each cis-element is 4bp or less from the previous one. Then complexcore score; which is the length of complex cis-elements of the CRMs are summed up for

each cis-element cluster. Motifscorer() elements calculates phasing score which is defined by how well consecutive cis-elements adhere to a 10.5x bp spacing relationship that allows binding of WUS molecules on the same side of the DNA. To normalize the phasing score, the phasing per base was calculated; where the phasing score is divided by the number of bp of the CRM.

These results are arranged by gene and by cluster into columns and printed out by Motifwriter(). This data is provided in Tables S6 and S7 as an excel and BED format. The data and viewing instructions are provided in the specified link. [https://github.com/Ado012/BasicCisElementAnalyzer]

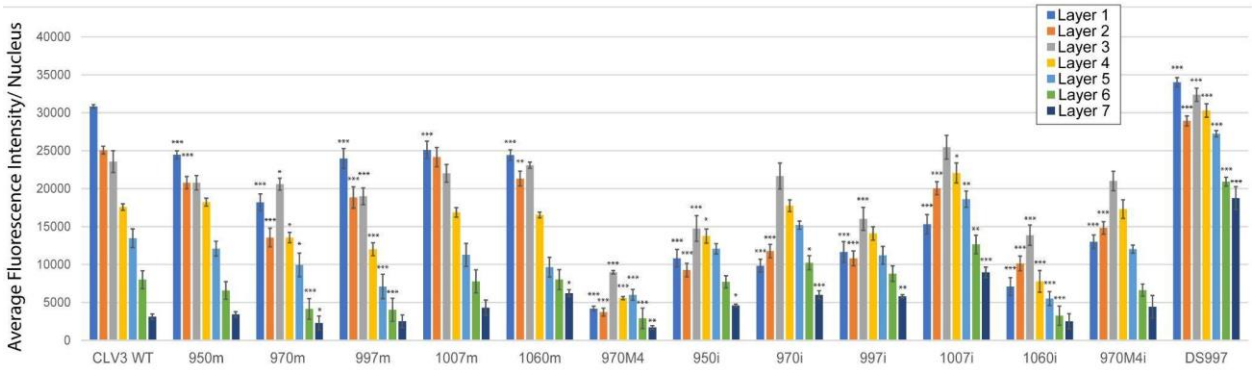

Fig. S1. Quantification of *pCLV3::H2B-mYFP* fluorescence levels in wild-type and various cis-element mutants.

Average fluorescence levels (mean ±S.E.) of H2B-mYFP in different cell layers of wild-type and various *pCLV3::H2b-mYFP* promoter variants indicated below each group. Mutation in single cis-elements (950M, 970M, 997M, 1007M, 1060M and 970M4), mutations in four of the five cis-element mutants [quadruple mutants-950i, 970i, 997i, 1007i, 1060i and 970M4i], and variant with doubled intervening distance between 970-997 and 997-1007 (DS-997). The error bars represent the standard error (n=4 biological replicates in all cases). * $p<0.05$, ** $p<0.01$, *** $p<0.001$

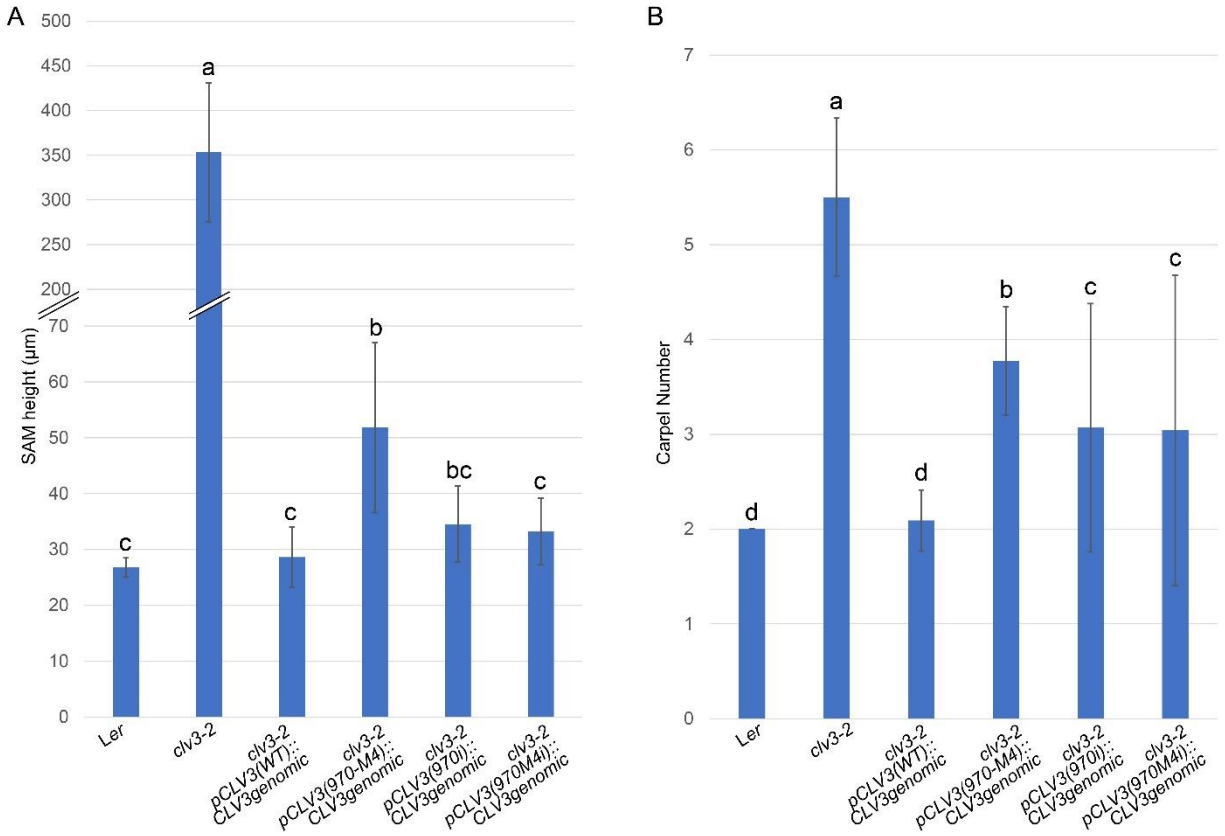

Fig. S2. Number and affinity of *CLV3* cis-elements determine the SAM and floral meristem complementation of *clv3* null mutants. (A) Average SAM height (mean ±S.D.) of wild-type, *clv3-2* mutants and various cis-element mutants of *pCLV3::CLV3* genomic constructs rescuing *clv3-2* mutants. (n=20, 2 plants from each of the ten independent transformed lines were considered). (B) Average number of carpels (mean ±S.D.) of the same genotypes described in (A). (n=10, 2 plants from each of a minimum of 5 independent transformed lines were considered). The different letter indicate the statistical difference between lines ($P<0.05$) as determined by Tukey's Honest Significant Difference (HSD) tests.

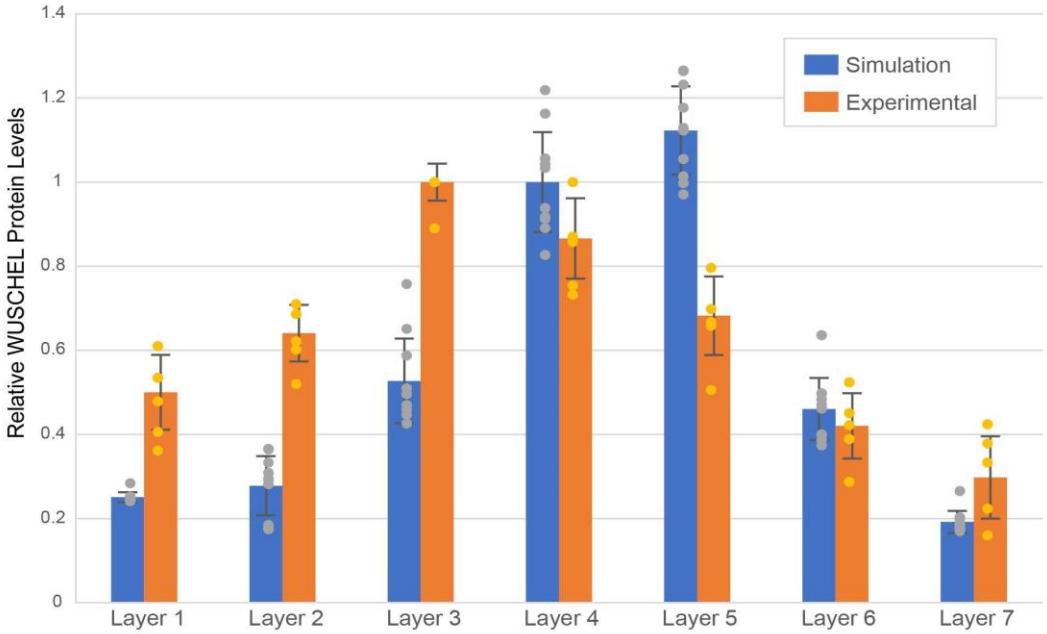

Fig. S3. Quantified WUS protein levels in different cell layers.

For the WUS levels in simulations, the ten cells with the highest WUS levels were selected for each cell layer. WUS levels for each cell were normalized to the cell with the highest WUS nuclear level (mean ±S.D.). For experimental quantification (orange), the average nuclear fluorescence levels for ten cells per layer of pWUS::eGFP-WUS were quantified from five independent SAMs (mean ±S.D.). WUS concentration in each cell layer was normalized by the mean of the layer with the highest WUS level.

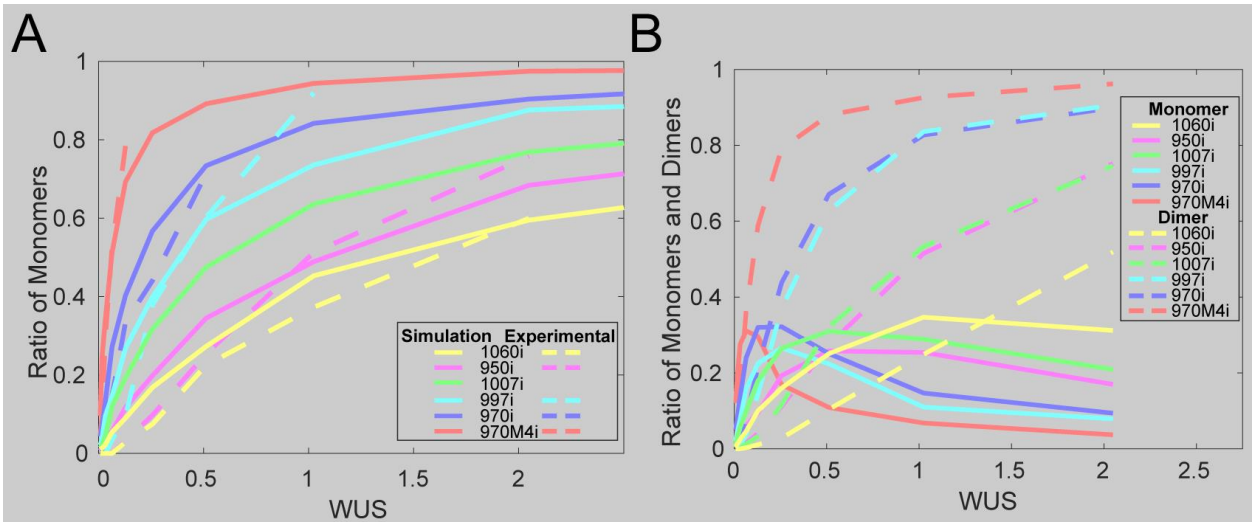

Fig. S4. Simulated WUS monomers and dimers at increasing WUS concentrations for various *CLV3* promoter variants.

(**A**) WUS monomers compared to the experimentally quantified data from EMSA. Solid lines represent simulation results and dashed lines represent values from EMSA data. (**B**) Simulated ratios of WUS monomers and dimers with increasing WUS concentrations. Solid lines represent WUS monomer species and dashed lines represent WUS dimers. The colored lines represent different *CLV3* cis-element mutants.

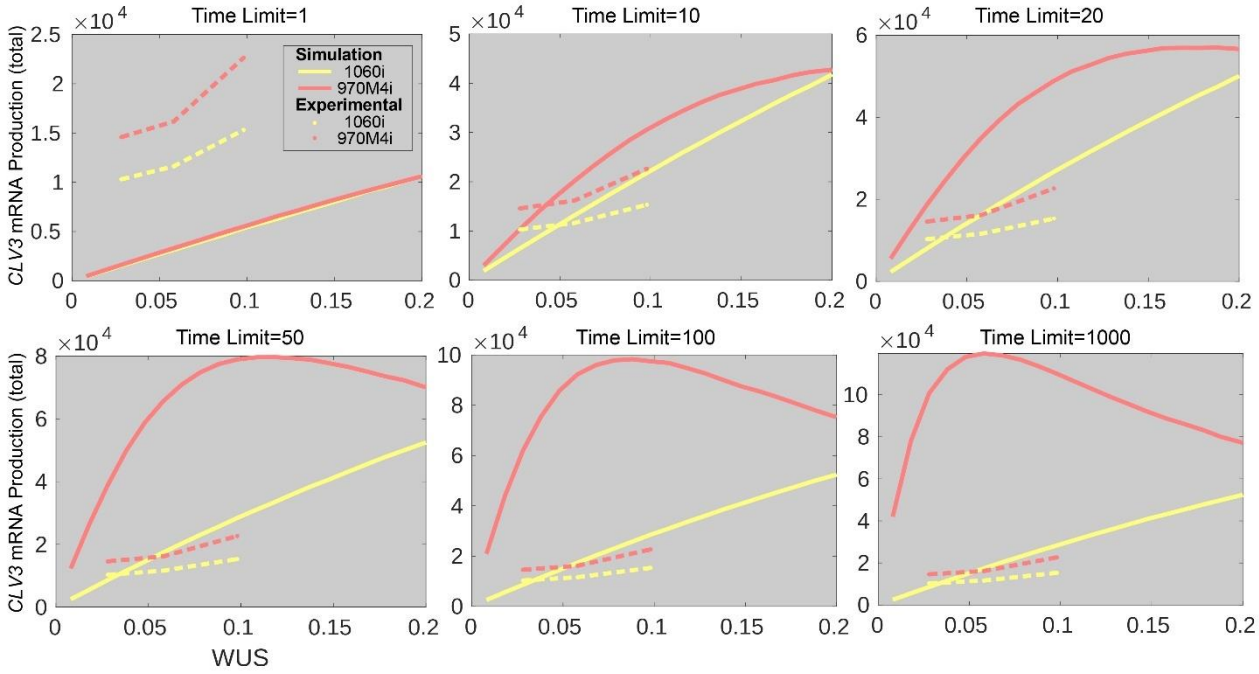

Fig. S5. The effect of WUS residence time limit on *CLV3* expression.

Scaled simulated values of *CLV3* mRNA production with increasing WUS concentrations is shown for the highest (970M4i [Solid red lines]) and the lowest (1060i [Solid yellow lines]) affinity cis-elements. The simulated data is compared to the *pCLV3::H2b-mYFP* levels in different cell layers shown as 3 dots (L1, L2 and L3) connected with dashed lines for 1060i (yellow) and 970M4i (red). Increasing the WUS residence time limit increases *CLV3* mRNA production and shifts the peak production to a lower WUS concentration range, especially in the case of higher affinity cis-element.

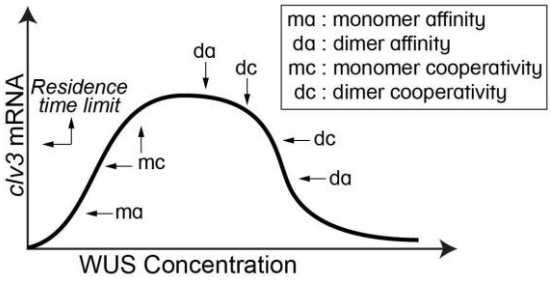

Fig. S6. The effect of RNA Pol II, WUS binding dynamics and WUS residence time limit on WUS concentration-dependent *CLV3* expression.

Increasing the affinity or cooperativity of WUS monomer leads to an increase in *CLV3* expression and shifts expression to a lower range of WUS concentration. Increasing the affinity or cooperativity of WUS dimer leads to *CLV3* repression, which decreases *CLV3* expression at high WUS concentration. Increasing the WUS residence time limit increases *CLV3* activation and shifts the activation to a lower range of WUS concentration.

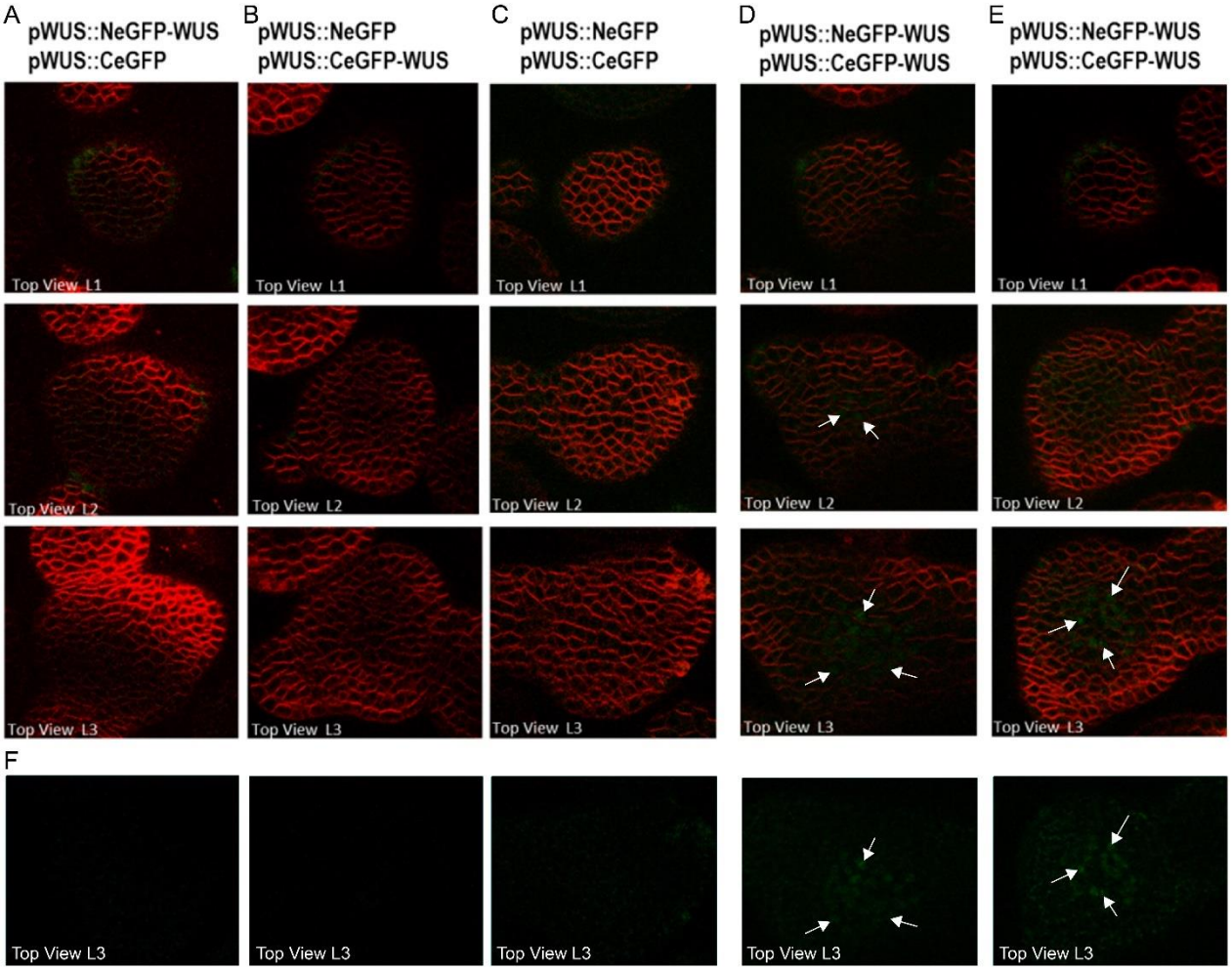

Fig. S7. *In planta* WUS protein homodimerization. The three rows represent the Z slices showing the Layer 1, Layer 2 and Layer 3 of SAM. (**A-E**) The WUS promoter was used to express all the BIFC construct in the wild-type background. (**A**) Plant expressing N' terminal fragment of eGFP translationally fused to WUS and C' terminal fragment of eGFP. (**B**) Plant expressing N' terminal fragment of eGFP and C' terminal fragment of eGFP translationally fused to WUS. (**C**) Plant expressing N' terminal fragment of eGFP and C' terminal fragment of eGFP. (**D** and **E**) Two independent lines expressing BiFC constructs of N' terminal fragment of eGFP translationally fused to WUS and C' terminal fragment of eGFP translationally fused to WUS. Arrows point to eGFP fluorescence (green) and FM4-64 staining is shown in red. (**F**) Images of Layer 3 shown in row 3, with the red channel turned off.

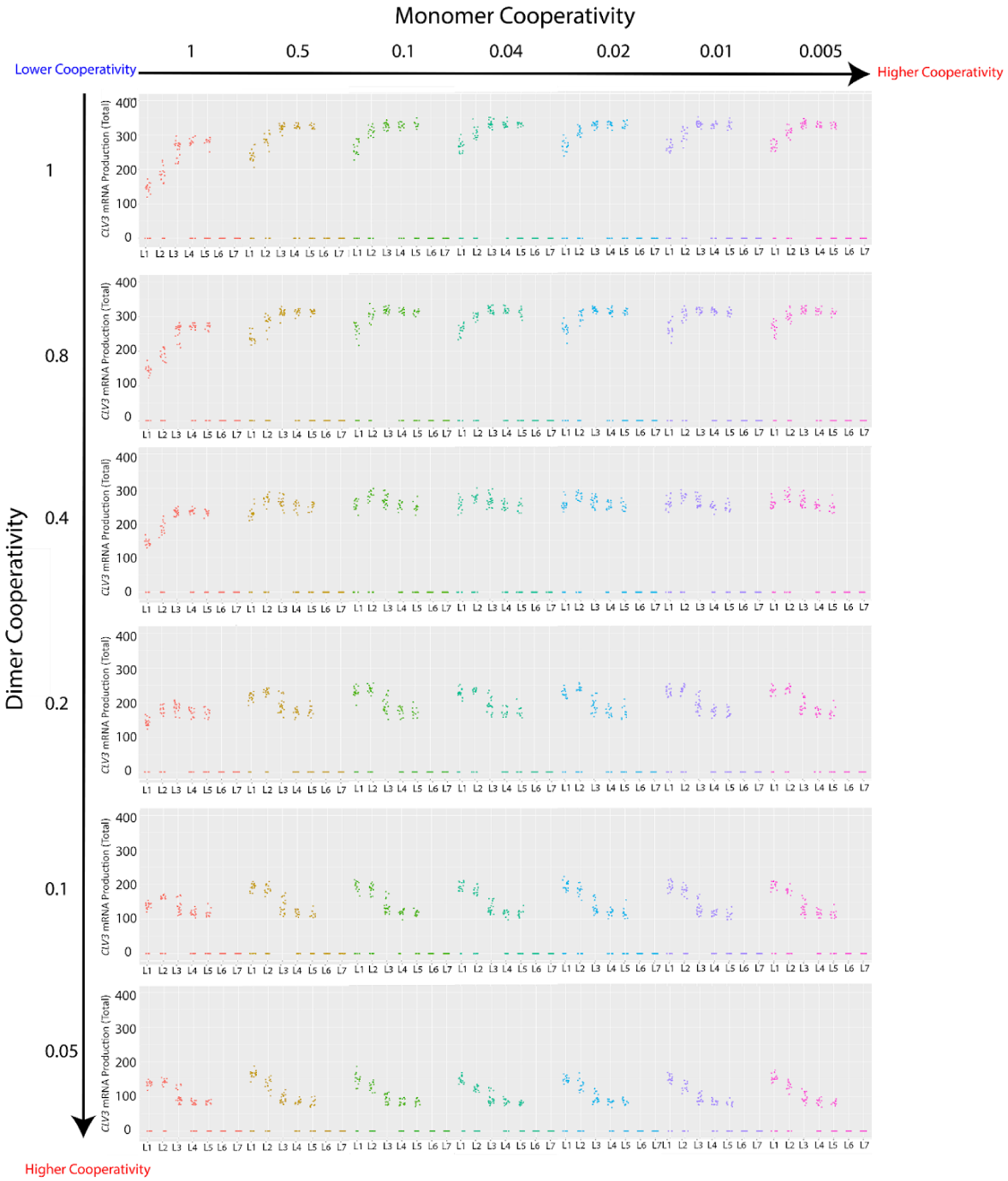

Fig. S8. Independent perturbations of the WUS monomer or dimer cooperativity.

The effect of changes in monomer cooperativity (from 1 to 0.005) and dimer cooperativity (from 1 to 0.05) on *CLV3* activation. The direction of the arrows indicate an increase in cooperativity. The result for each combination of monomer and dimer cooperativity value is represented by the graph at their intersection. The individual graphs represent the *CLV3* activation in different cell layers (L1 to L7) of simulated SAMs under the cooperativity levels noted for each simulation. The dots represent the values of the *CLV3* signal for individual simulated cells.

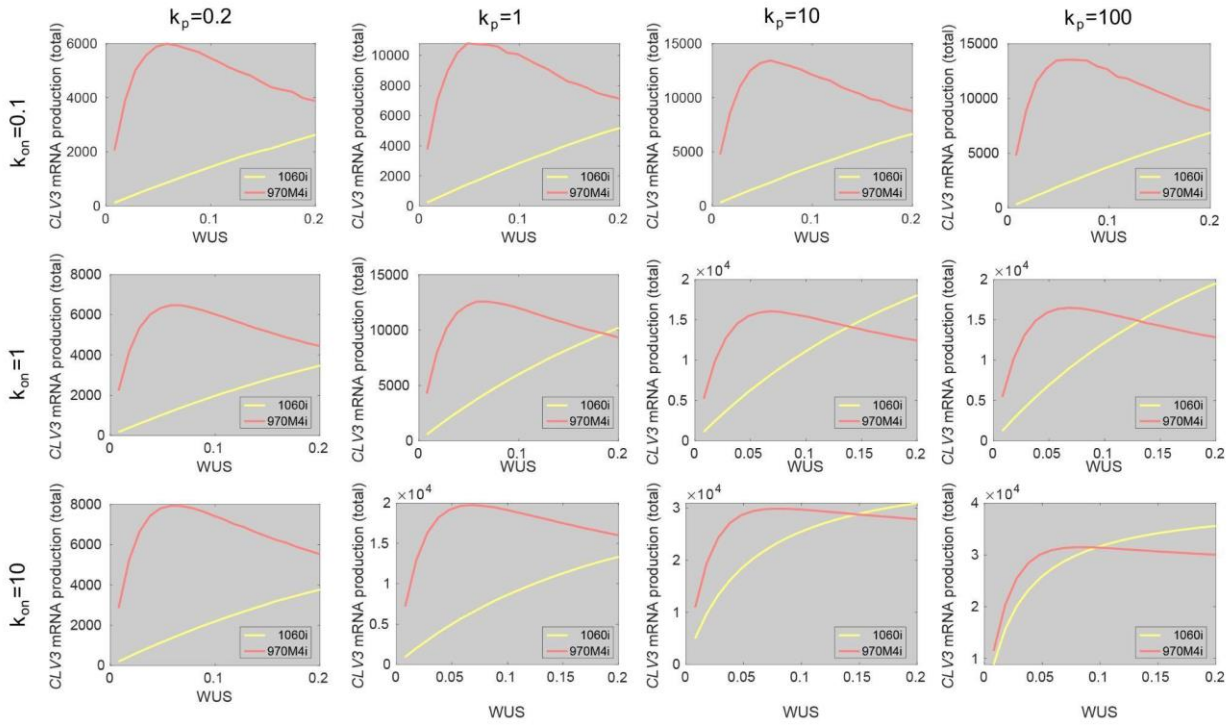

Fig. S9. Sensitivity analysis showing the effect of different k_{on}, k_p values on the behavior of highest and lowest affinity single cis-elements.

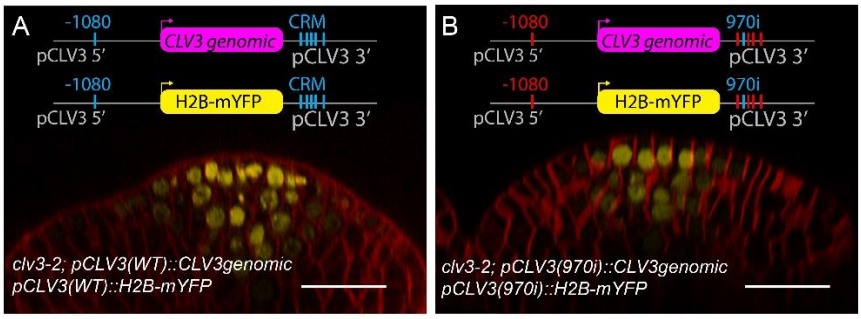

Fig. S10. Reactivation of mutant *CLV3* promoter (970i) in *clv3* complemented background. (**A**) *clv3-2* mutants complemented with the wild-type CLV3 promoter expressing *CLV3* genomic sequence [*pCLV3(WT)::CLV3* genomic]and showing the wild-type *CLV3* reporter [*pCLV3(WT)::H2B-mYFP*] expression. (**B**) *clv3-2* mutants complemented with the 970i *CLV3* promoter expressing *CLV3* genomic [*pCLV3(970i)::CLV3* genomic] sequence and showing the 970i *CLV3* reporter [*pCLV3(970i)::H2B-mYFP*]. Scale bar = 20 μm.

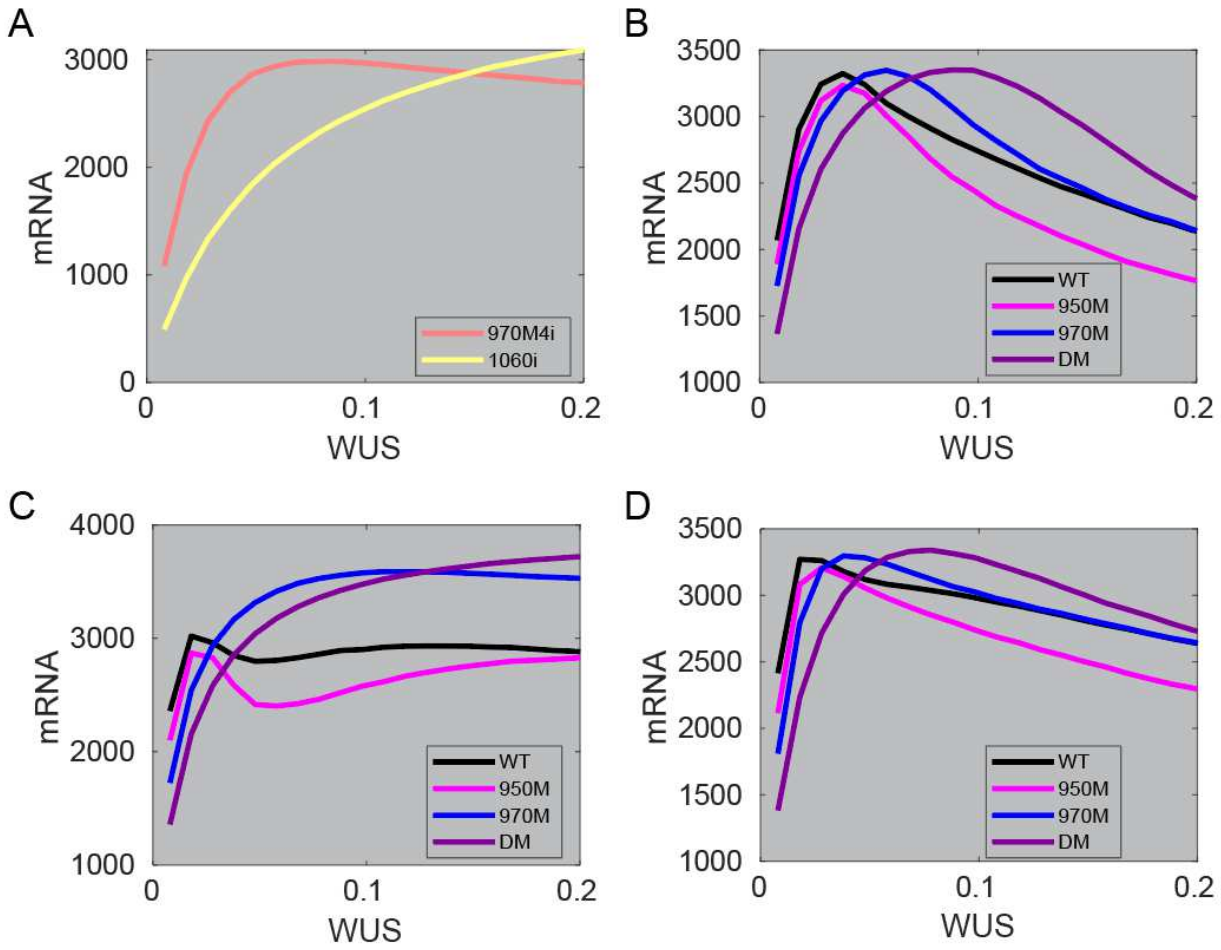

Fig. S11. Single cell simulation results of WUS mediated activation of *CLV3* by using fast dynamics (k_{on}=10 and k_p=10). (**A**) Single cis-element behavior for 970M4i and 1060i. (**B**) Multiple cis-element behaviors with low cooperativity between neighboring cis-elements only. (**C**) Multiple cis-element behaviors with distance dependent cooperativity. (**D**) Multiple cis-element behaviors with high cooperativity between neighboring cis-elements only.

Table S1. Experimentally derived KD values from EMSA.

K_d Values for the DNA binding domain of WUS to cis-elements probes were obtained from (*24*).

Parameter	Value	Definition	Unit
K_d	0.05830	Dissociation constant of 970M4i	μM
K_d	0.9571	Dissociation constant of 950i	μM
K_d	0.1855	Dissociation constant of 970i	μM
K_d	0.3663	Dissociation constant of 997i	μM
K_d	0.5652	Dissociation constant of 1007i	μM
K_d	1.249	Dissociation constant of 1060i	μM

Table S2. Parameter Values Used in Single Cell Model.

All values in this table were calibrated in this model.

Parameter	Value	Definition	Unit
k_p	0.2-100	Pol II binding rate	$\mu M^{-1}s^{-1}$
k_{on}	0.1-10	Monomer, dimer binding rate	$\mu M^{-1}s^{-1}$
t_{delay}	4	Time delay for the recruitment of successive Pol II	s
a_m	1.1	Parameter determining the level of monomer cooperativity	-
b_m	50	Parameter determining the distance threshold of monomer cooperativity	$2bp$
a_d	1.1	Parameter determining the level of dimer cooperativity	-
b_d	50	Parameter determining the distance threshold of dimer cooperativity	$2bp$
RTL	10	Residence time limit	s
t_{final}	1.6×10^6	Final time of a simulation	s
a_c	0.3	Parameter determining the nonlinearity of the distance function for the cooperativity	-

Table S3. *CLV3* mRNA Production Parameters used in the 3D cell-based model.

Parameter	Value	Definition	Unit	Reference
clv3CLV3P	3.0	Rate of *CLV3* mRNA production	s^{-1}	Calibrated in model
clv3SourceWidth	3	Radius of *CLV3* activation domain in x-y plane	a.u.	Experimentally determined
clv3WusSatPoint	425	Maximum effective WUS concentration	-	Calibrated in model
clv3CooptMonEffect	0.01	Parameter determining the level of monomer cooperativity	-	Calibrated in model
clv3CooptDimEffect	0.20	Parameter determining the level of dimer cooperativity	-	Calibrated in model
polTimeLimit	5	Time delay for Pol II firing	s	Experimentally determined
n_{970}	3	The minimal exponent in the cooperativity associated with 970	-	Calibrated in model
k_p	0.1	Pol II binding parameter (*clv3polBaseBindAffinity*)	s^{-1}	Calibrated in model

Table S4. Primers used in this study.

Construct	Primer Name	Sequence
CLAVATA3 mutant promoter		
pCLV3 950M	Fwd	CGTACCCCCAAATTTTCCCAACGGTACATTGC
pCLV3 950M	Rev	TTTTCAATTGTCAATGCAAATACCCCATGG
pCLV3 970M	Fwd	GGTATTTGCATTGACAATTGAAAACGTAC
pCLV3 970M	Rev	CCATGGATGTGATAGTCACAATTAAAC
pCLV3 997M	Fwd	GTGACTATCACATCCATTAATTATTTGC
pCLV3 997M	Rev	AATGGAACATACAATAATAAAAATGATGATG
pCLV3 1007M	Fwd	GATTCGATGATGTGGTGGGAAGG
pCLV3 1007M	Rev	ATCATCATCATTTTTGGGGTTGTATGTT
pCLV3 1060M	Fwd	GTCGGTTCCCCTTATCCTTCCCACCACATCATC
pCLV3 1060M	Rev	TTTGGGGCAGTGACAGGCAGTGTCAGTG
Double Space Around 997 primers		
pCLV3 DS-C	Rev	TTATTATTGTATGTTTTGTATGTTTAATTGTGACTATCAC ATCCTGTGACTATCACATCC
pCLV3 RB	Fwd	ATAAAAAAATGATGATGATGATTCGATGATGTGGTGGG AAG
EMSA probes		
Cis-element	**Orientation**	**Sequence**
970	Fwd	CAATTGTCAATGCAAATAATTAATGGATGTG
970	Rev	CACATCCATTAATTATTTGCATTGACAATTG
997	Fwd	TTATTGTATGTTTAATTGTGACTAT
997	Rev	ATAGTCACAATTAAACATACAATAA
970+997	Fwd	CAATTGTCAATGCAAATAATTAATGGATGTGATAGTCAC AATTAAACATACAATA
970+997	Rev	TATTGTATGTTTAATTGTGACTATCACATCCATTAATTAT TTGCATTGACAATTG

970m+997	Fwd	CAATTGTCAATGCAAAGGGGGGGGGATGTGATAGTCA CAATTAAACATACAATA
970m+997	Rev	TATTGTATGTTTAATTGTGACTATCACATCCCCCCCCCCT TTGCATTGACAATTG
970+997m	Fwd	CAATTGTCAATGCAAATAATTAATGGATGTGATAGTCAC AGGGGAACATACAATA
970+997m	Rev	TATTGTATGTTCCCCTGTGACTATCACATCCATTAATTAT TTGCATTGACAATTG
970M4+997	Fwd	CAATTGTCAATGCAAATAACTAATGGATGTGATAGTCAC AATTAAACATACAATA
970M4+997	Rev	TATTGTATGTTTAATTGTGACTATCACATCCATTAGTTAT TTGCATTGACAATTG
970M4+997m	Fwd	CAATTGTCAATGCAAATAACTAATGGATGTGATAGTCAC AGGGGAACATACAATA
970M4+997m	Rev	TATTGTATGTTCCCCTGTGACTATCACATCCATTAGTTAT TTGCATTGACAATTG
Double Space 970+997	Fwd	CAATTGTCAATGCAAATAATTAATGGATGTGATAGTCAC AGGATGTGATAGTCACAATTAAACATACAATA
Double Space 970+997	Rev	TATTGTATGTTTAATTGTGACTATCACATCCTGTGACTAT CACATCCATTAATTATTTGCATTGACAATTG
BiFC Cloning		
ΔCeGFP	NeGFP -Fw	GGATCCATGGAGCCGCCACAGCATCAG
	NeGFP-Rev	GGCCATGATATAGACGTTGTGGCTGTTG
ΔNeGFP	CeGFP-Fw	GACAAGCAGAAGAACGGCATCAAGGTG
	CeGFP-Rev	CATGGCGCGCCATGGTGAAGGAGCCCTG
ΔWUS	ΔWUS-Fw	TGAACTAGGCCTGCAAGGGCG
	ΔWUS-Rev	GGATCCCTTGTACAGCTCGTC

1502

Table S5. Cis-element mutant sequence library.

CLV3 Promoter name	Sequence
WT	5'tttATTAgtacgttttcaattgtcaatgcaaaTAATTAATggatgtgatagtcacaATTAaa catacaaTAATaaaaatgatgatgatgattcgatgatgtggtgggaaggataaATTAaa-3'
950M	5'tttGGGGgtacgttttcaattgtcaatgcaaaTAATTAATggatgtgatagtcacaATTAaa catacaaTAATaaaaatgatgatgatgattcgatgatgtggtgggaaggataaATTAaa-3'
970M	5'tttATTAgtacgttttcaattgtcaatgcaaaTACCCCATggatgtgatagtcacaATTAaa catacaaTAATaaaaatgatgatgatgattcgatgatgtggtgggaaggataaATTAaa-3'
997M	5'tttATTAgtacgttttcaattgtcaatgcaaaTAATTAATggatgtgatagtcacaATGGaa catacaaTAATaaaaatgatgatgatgattcgatgatgtggtgggaaggataaATTAaa-3'
1007M	5'tttATTAgtacgttttcaattgtcaatgcaaaTAATTAATggatgtgatagtcacaATTAaa catacaaCCCCaaaaatgatgatgatgattcgatgatgtggtgggaaggataaATTAaa-3'
1060M	5'tttATTAgtacgttttcaattgtcaatgcaaaTAATTAATggatgtgatagtcacaATTAaa catacaaTAATaaaaatgatgatgatgattcgatgatgtggtgggaaggataaGGGGaa-3'
970M4	5'tttATTAgtacgttttcaattgtcaatgcaaaTAACTAATggatgtgatagtcacaATTAaa catacaaTAATaaaaatgatgatgatgattcgatgatgtggtgggaaggataaATTAaa-3'
950i	5'tttATTAgtacgttttcaattgtcaatgcaaaTACCCCATggatgtgatagtcacaATGGaa catacaaCCCCaaaaatgatgatgatgattcgatgatgtggtgggaaggataaGGGGaa-3'
970i	5'tttGGGGgtacgttttcaattgtcaatgcaaaTAATTAATggatgtgatagtcacaATGGaa catacaaCCCCaaaaatgatgatgatgattcgatgatgtggtgggaaggataaGGGGaa-3'
997i	5'tttGGGGgtacgttttcaattgtcaatgcaaaTACCCCATggatgtgatagtcacaATTAaa catacaaCCCCaaaaatgatgatgatgattcgatgatgtggtgggaaggataaGGGGaa-3'
1007i	5'tttGGGGgtacgttttcaattgtcaatgcaaaTACCCCATggatgtgatagtcacaATGGaa catacaaTAATaaaaatgatgatgatgattcgatgatgtggtgggaaggataaGGGGaa-3'
1060i	5'tttGGGGgtacgttttcaattgtcaatgcaaaTACCCCATggatgtgatagtcacaATGGaa catacaaCCCCaaaaatgatgatgatgattcgatgatgtggtgggaaggataaATTAaa-3'
970M4i	5'tttGGGGgtacgttttcaattgtcaatgcaaaTAACTAATggatgtgatagtcacaATGGaa catacaaCCCCaaaaatgatgatgatgattcgatgatgtggtgggaaggataaGGGGaa-3'

Data S1. (separate file)

Individual data points, means, N and P values are arranged by figure and panel.